Cell Reports

Article

Genome-wide CRISPR-Cas9 knockout library screening identified PTPMT1 in cardiolipin synthesis is crucial to survival in hypoxia in liver cancer

Graphical Abstract

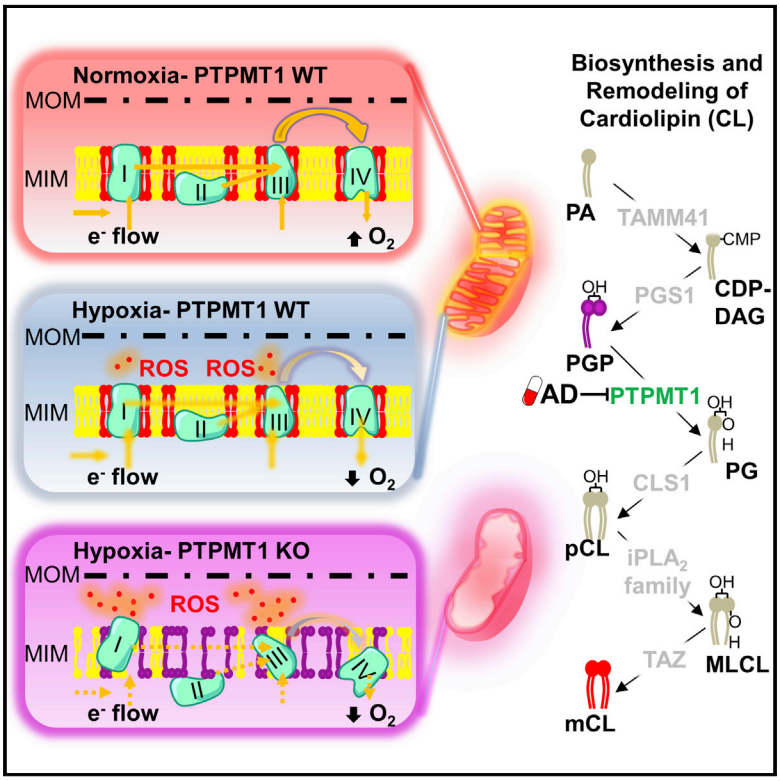

Highlights

- CRISPR-Cas9 library screen identifies that PTPMT1 is a vital gene for hypoxic survival
- PTPMP1 synthesizes CL to trap electrons at mitochondria to prevent ROS buildup
- Knockout or inhibition of PTPMT1 induces ROS and apoptosis in hypoxic cancer cells
- PTPMT1 is a targetable metabolic vulnerability to combat hypoxic solid tumors

Authors

Macus Hao-Ran Bao, Chunxue Yang, Aki Pui-Wah Tse, ..., Clive Yik-Sham Chung, Chun-Ming Wong, Carmen Chak-Lui Wong

Correspondence

jackwong@pathology.hku.hk (C.-M.W.), carmencl@pathology.hku.hk (C.C.-L.W.)

In Brief

Bao et al. use CRISPR library screening to identify PTPMT1, an important gene for hypoxic survival of HCC cells. PTPMT1 synthesizes cardiolipin, a crucial component of mitochondrial membrane, to maintain mitochondrial integrity, trap electrons, and prevent excessive ROS accumulation under hypoxia. PTPMT1 is a targetable vulnerability to combat hypoxic cancers.

Bao et al., 2021, Cell Reports *34*, 108676
January 26, 2021
https://doi.org/10.1016/j.celrep.2020.108676

CellPress

Cell Reports

CellPress
OPEN ACCESS

Article

Genome-wide CRISPR-Cas9 knockout library screening identified PTPMT1 in cardiolipin synthesis is crucial to survival in hypoxia in liver cancer

Macus Hao-Ran Bao,[1,4] Chunxue Yang,[1,4] Aki Pui-Wah Tse,[1,4] Lai Wei,[1,4] Derek Lee,[1,4] Misty Shuo Zhang,[1] Chi Ching Goh,[1] David Kung-Chun Chiu,[1] Vincent Wai-Hin Yuen,[1] Cheuk-Ting Law,[1] Wai-Ching Chin,[1] Noreen Nog-Qin Chui,[1] Bowie Po-Yee Wong,[1] Cerise Yuen-Ki Chan,[1] Irene Oi-Lin Ng,[1,2] Clive Yik-Sham Chung,[1,3] Chun-Ming Wong,[1,2,*] and Carmen Chak-Lui Wong[1,2,5,*]

[1]Department of Pathology, The University of Hong Kong, Hong Kong
[2]State Key Laboratory of Liver Research, The University of Hong Kong, Hong Kong
[3]School of Biomedical Sciences, The University of Hong Kong, Hong Kong
[4]These authors contributed equally
[5]Lead contact
*Correspondence: jackwong@pathology.hku.hk (C.-M.W.), carmencl@pathology.hku.hk (C.C.-L.W.)
https://doi.org/10.1016/j.celrep.2020.108676

SUMMARY

Hypoxia, low oxygen (O_2), is a key feature of all solid cancers, including hepatocellular carcinoma (HCC). Genome-wide CRISPR-Cas9 knockout library screening is used to identify reliable therapeutic targets responsible for hypoxic survival in HCC. We find that protein-tyrosine phosphatase mitochondrial 1 (PTPMT1), an important enzyme for cardiolipin (CL) synthesis, is the most significant gene and ranks just after hypoxia-inducible factor (HIF)-1α and HIF-1β as crucial to hypoxic survival. CL constitutes the mitochondrial membrane and ensures the proper assembly of electron transport chain (ETC) complexes for efficient electron transfer in respiration. ETC becomes highly unstable during hypoxia. Knockout of PTPMT1 stops the maturation of CL and impairs the assembly of ETC complexes, leading to further electron leakage and ROS accumulation at ETC in hypoxia. Excitingly, HCC cells, especially under hypoxic conditions, show great sensitivity toward PTPMT1 inhibitor alexidine dihydrochloride (AD). This study unravels the protective roles of PTPMT1 in hypoxic survival and cancer development.

INTRODUCTION

Hepatocellular carcinoma (HCC), primary liver cancer as a result of hepatocyte transformation, is the fourth most common and second most fatal cancer worldwide. The continuous dismal outcome of HCC is due to a combination of reasons, including difficulties for early detection, the lack of guaranteed curative treatment, and high recurrence rate. To date, the only FDA (U.S. Food and Drug Administration)-approved therapies for advanced HCC patients include tyrosine kinase inhibitors (TKIs) and an immune checkpoint inhibitor, Nivolumab. TKIs, in general, could only extend the survival of HCC patients for about 3–6 months, whereas immune checkpoint inhibitors display responsive rates of only about 20% (Bruix et al., 2017; El-Khoueiry et al., 2017; Llovet et al., 2008).

Hypoxia, oxygen (O_2) deprivation, frequently occurs in solid cancers due to the lack of blood supply. Cellular adaptation to hypoxia mainly relies on the transcription factor, hypoxia-inducible factor (HIF), a heterodimer consisting of an O_2-labile HIF-1/2α subunit and a constitutively expressed HIF-1β subunit (Semenza, 2012). With O_2 (normoxia), prolyl hydroxylase (PHD) hydroxylates HIF-1/2α at specific proline residues (Epstein et al., 2001), supporting the recognition and binding of E3 ubiquitin ligase von Hippel-Lindau protein (VHL) to drive the proteasomal degradation of HIF-1/2α (Kaelin and Ratcliffe, 2008). Without O_2, the PHD/VHL-mediated protein degradation is blocked. Stabilized HIF-1/2α proteins translocate to the nucleus to dimerize with HIF-1β and bind to genes with -A/GCGTG-, hypoxia response elements (HREs), to initiate the transcriptional cascades (Wang et al., 1995).

HIFs induce a panel of genes for metabolic reprogramming, metastasis, angiogenesis, and chemo- and radio-resistance (Semenza, 2012). In the presence of O_2, cells convert glucose to pyruvate and then to acetyl-coenzyme A (CoA) to initiate the tricarboxylic acid (TCA) cycle in the mitochondrion. NADH, a source of electrons, is produced along the way. The electron is passed sequentially to 4 different complexes located in the electron transport chain (ETC; respiratory chain) and finally to O_2. This process is known as oxidative phosphorylation (OXPHOS), generating 36 ATPs per glucose. When O_2 becomes limited, electrons could not be fully absorbed due to the lack of electron recipient, leading to reactive oxygen species (ROS) accumulation in the ETC. ROS attack different cellular components such as DNA and cell membrane, causing apoptosis and cell-cycle

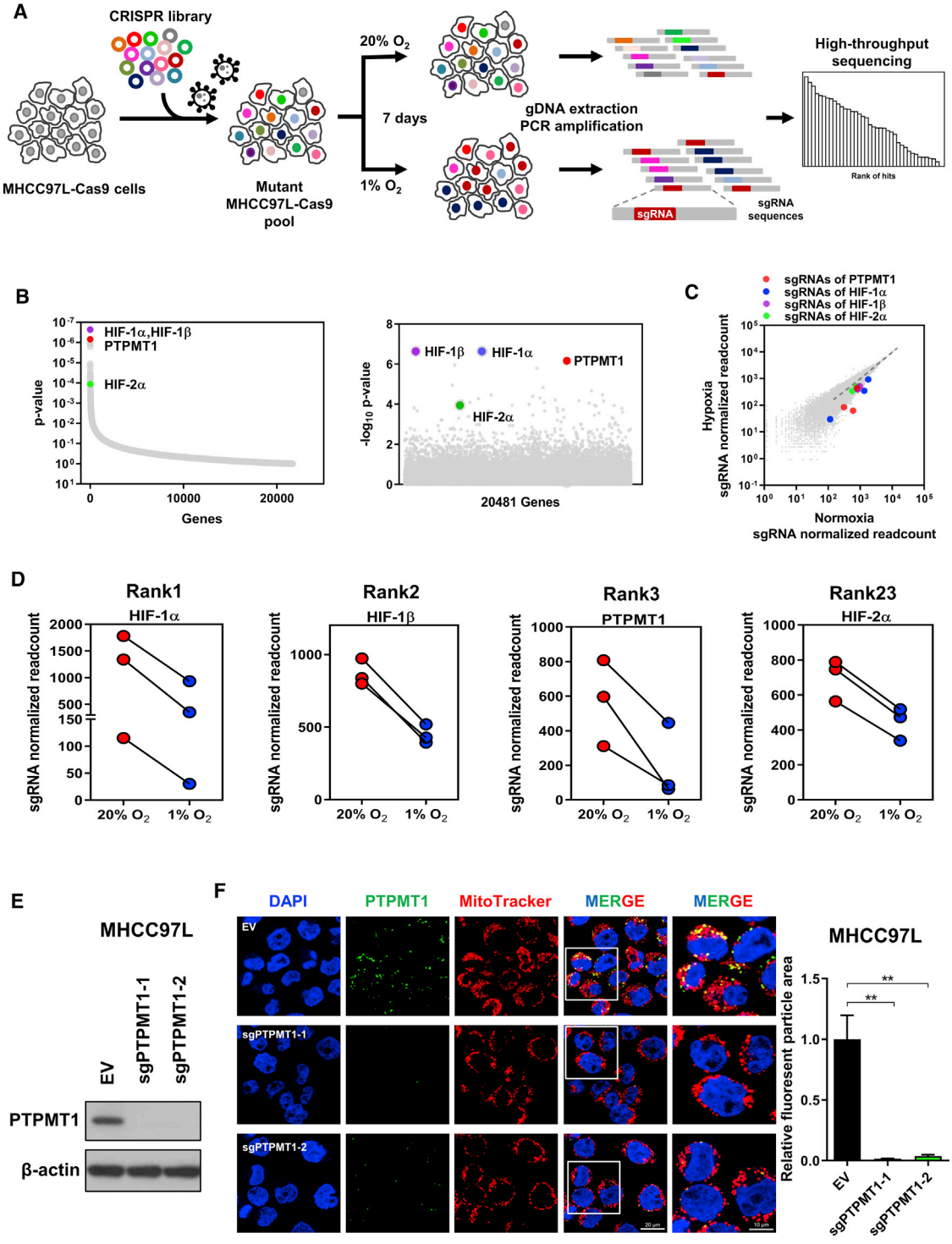

Figure 1. Identification of PTPMT1 by CRISPR-Cas9 library screening for HCC cell hypoxic survival

(A) Schematic diagram showing the workflow of the genome-wide CRISPR-Cas9 KO library screening. The human genome-wide CRISPR-Cas9 KO pooled library (GeCKO v2A library) with 65,386 sgRNAs was transduced into MHCC97L-Cas9 at a low multiplicity of infection (MOI). A mutant cell pool was generated by puromycin selection for 7 days. The mutant cells were cultured in 20% O_2 or 1% O_2 for 7 days. Genomic DNA (gDNA) of normoxic and hypoxic mutant cells were extracted, and the sgRNAs were amplified by PCR. Copy numbers of sgRNAs were determined by high-throughput sequencing and analyzed by MAGeCK v0.5.7 algorithm.

(B) HIF-1α (blue dot), HIF-1β (purple dot), PTPMT1 (pink dot), and HIF-2α (green dot) were ranked as the first, second, third, and 23rd most important genes from the library screening for hypoxic survival.

(legend continued on next page)

arrest. HIFs allow cells to adapt through inducing genes (LDHA and PDK1) that could divert pyruvate into lactate instead of acetyl-CoA so that energy could be generated by glycolysis to minimize OXPHOS (Semenza, 2012). Earlier hypotheses posit that mitochondria are being degraded under hypoxic conditions so that ROS could not be produced and macromolecules from mitochondria could be recycled to support cell survival (Semenza, 2012). However, compelling evidence converges to prove that mitochondria are not completely shut down during hypoxia. HIFs induce the less active subunits NDUFA4L2 and COX4-2 in complexes I and IV, respectively, to decelerate electron flow in the ETC to alleviate ROS level (Fukuda et al., 2007; Lai et al., 2016; Tello et al., 2011). We speculated that, if the ETC complexes are not assembled properly when the O_2 level declines, the ROS level would be even higher, as the electrons have no way to be transferred in the mitochondria.

Given the clinical importance of hypoxia in HCC, knowledge about the molecular consequences supporting cellular adaptation in hypoxia is warranted. Comparison of transcriptomic profiles between normoxic and hypoxic cells is, by far, the most common approach to identify genes related to hypoxia. However, this approach has drawbacks. First, a large number of genes are induced by hypoxia, and genes with the highest induction may not be the genes with the greatest biological importance for hypoxic adaptation. Second, genes important for hypoxic survival may not be necessarily induced by hypoxia or regulated by HIFs. Recently, the CRISPR (clustered regularly interspaced short palindromic repeat)-Cas9 knockout (KO) library screening has been reported as a powerful forward genetic screening approach to identify genes responsible for their associated biological activities. The CRISPR-Cas9 has been adapted for genome-wide screening with a pooled guide RNA library to identify molecular mechanisms underlying cancer cell survival, metastasis, and drug resistance in various models (Shalem et al., 2015; Zhou et al., 2014).

In this study, we performed the genome-wide CRISPR-Cas9 KO library (GeCKO v2A library) screening and identified PTPMT1 (protein-tyrosine phosphatase mitochondrial 1), an important enzyme for cardiolipin (CL) synthesis as the third most significant gene for hypoxic adaptation, ranking right after HIF-1α and HIF-1β. PTPMT1 is a phosphatase that removes a phosphate group from phosphatidylglycerol (PG) phosphate (PGP) to generate PG. which later dimerizes to become CL precursor. CL is a major component of the mitochondria membranes. Controversial to the traditional understanding that mitochondria are ''useless'' in hypoxia, we hypothesize that mitochondrial integrity is essential to cell survival in hypoxia, as complete elimination of mitochondria would lead to inefficient electron transfer and instant accumulation of ROS, which causes cell death. In this study, we delineated the metabolic advantages of PTPMT1 in hypoxic cells and highlighted its clinical relevance and therapeutic implications in HCC and in other solid cancers. This knowledge will shed light on the development of therapeutic strategies targeting hypoxic HCC cells and other cancer cells.

RESULTS

Genome-wide CRISPR-Cas9 KO library screening in cancer cells identified PTPMT1 as an essential gene for survival in hypoxia

We carried out an unbiased genome-wide CRISPR-Cas9 KO library screening to investigate the molecular basis that enables HCC cells to adapt and survive in hypoxia. The HCC cell line MHCC97L, which stably expressed Cas9 protein, was established by lentiviral approach (Figure 1A). The human GeCKO v2A library, comprising 65,386 unique single-guide RNAs (sgRNAs) targeting 19,052 protein-coding genes and 1,864 microRNAs, was transduced into MHCC97L-Cas9 cells with low viral titers to ensure that each cell took up one sgRNA (Barrangou et al., 2007). A mutant cell pool was established after puromycin selection. Next, we cultured the mutant cell pool in normoxia (20% O_2) and hypoxia (1% O_2) for 7 days (Figure 1A). We posited that KO of genes essential for hypoxic survival will sensitize HCC cells to hypoxia-induced cell death. Under hypoxia, HCC cells carrying sgRNAs targeting hypoxic survival genes were negatively selected and depleted in the mutant cell pool. The copy numbers of sgRNAs were quantified by high-throughput sequencing after genomic DNA (gDNA) extraction and amplification. After hypoxic selection, we achieved around 400× coverage of the library with 95% of the sgRNA sequences retained in all samples (Figures S1A and S1B). This confirms that the read depth and library coverage for the CRISRP-Cas9 library screening are sufficient (Figures S1A and S1B). This screening showed that a subset of guide RNAs (gRNAs) targeting 264 genes was significantly depleted ($p < 0.01$) in the hypoxic cells as compared to that in normoxic cells (NCBI: PRJNA673757). Gene set enrichment analysis (GSEA) revealed that these negatively selected genes were significantly enriched in cancer hallmarks, including Myc targets, OXPHOS, glycolysis, and hypoxia response, highlighting that these genes confer HCC cell survival advantages in hypoxia (Figure S1C). Using the MAGeCK algorithm, we identified HIF-1α (rank 1) and HIF-1β (rank 2) as the two most essential genes for hypoxic adaptation. HIF-2α (rank 23) was also found as a top gene in the screening. These positive control genes demonstrated the reliability of the screening. More interestingly, PTPMT1 was ranked the third most important gene following right after HIF-1α and HIF-1β (Figures 1B–1D). All

(C) The copy numbers of sgRNAs in normoxic and hypoxic mutant cells are strongly correlated. The sgRNAs of HIF-1α, HIF-1β, PTPMT1, and HIF-2α were decreased in hypoxic conditions.
(D) Depletion of sgRNAs targeting HIF-1α, HIF-1β, PTPMT1, and HIF-2α in a hypoxic mutant cell pool.
(E) PTPMT1 protein levels of MHCC97L-Cas9-EV, -sgPTPMT1-1, and -sgPTPMT1-2 subclones were determined by western blotting.
(F) Left: immunofluorescence (IF) staining images of MHCC97L-Cas9-EV, -sgPTPMT1-1, and -sgPTPMT1-2 subclones (scale bar, 20 μm). Magnified merged images show localization of PTPMT1 at the mitochondria (scale bar, 10 μm). Right: quantification of relative fluorescence.
Error bars indicate mean ± SEM (n = 3). *$p < 0.05$, Student's t test.
See also Figure S1.

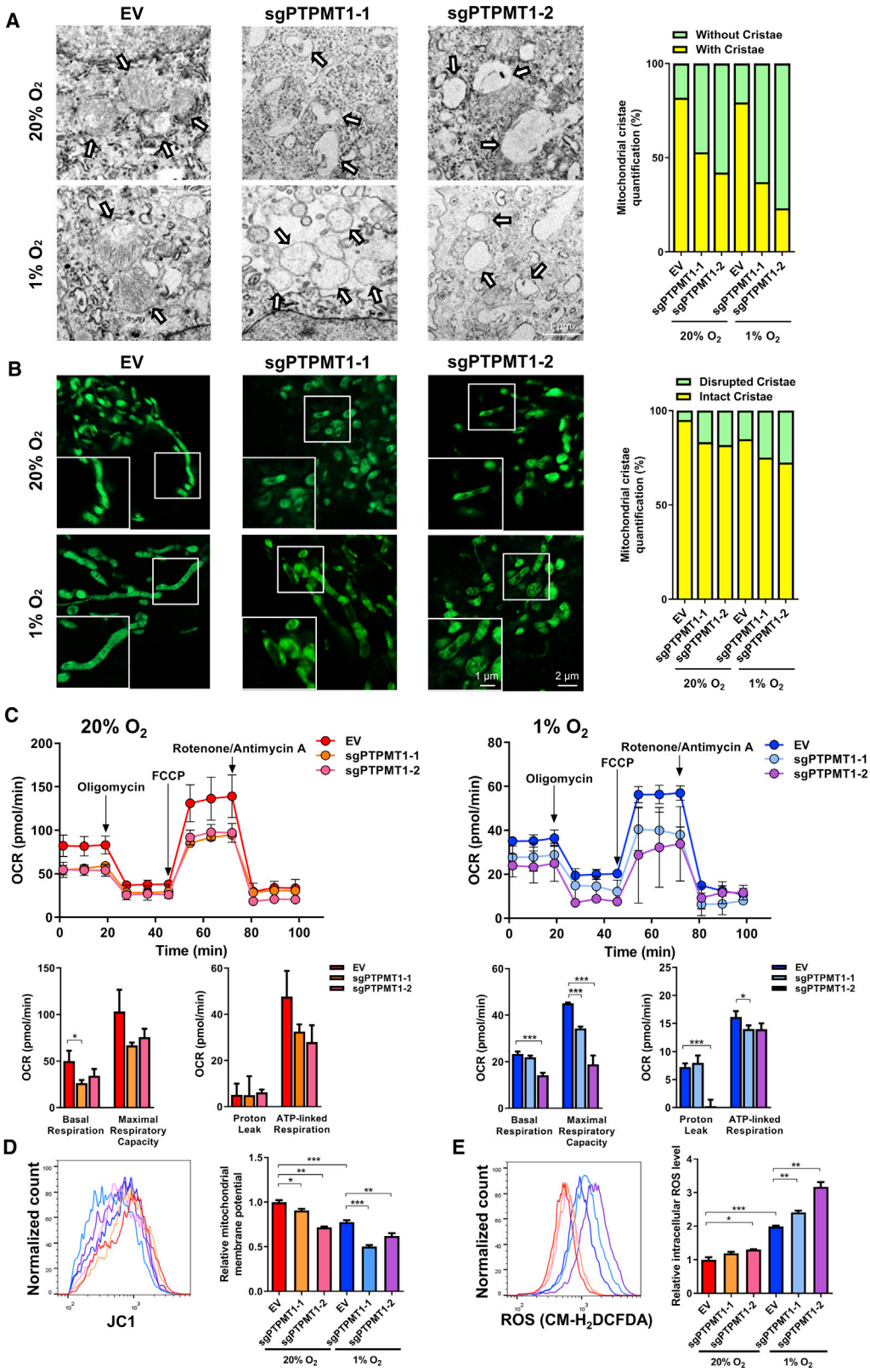

(legend on next page)

sgRNAs targeting HIF-1α, HIF-1β, HIF-2α, and PTPMT1 were dramatically depleted by hypoxia (Figure 1D).

KO of PTPMT1 drastically induced oxidative stress in hypoxic cancer cells

The importance of the HIF-1 complex in hypoxic adaptation is well established, whereas the biological roles of PTPMT1 in hypoxic adaptation and cancer development have not been elucidated. We generated PTPMT1 KO stable subclones using the CRISPR-Cas9-KO system in cancer cell lines including MHCC97L (human HCC) and Hepa1-6 (mouse HCC). Western blotting clearly indicated the successful PTPMT1 KO in the HCC cell lines (Figures 1E and S1D). Quantitative real-time PCR and western blotting showed that PTPMT1 expression was not induced by hypoxia, suggesting that hypoxic survival genes might not be necessarily hypoxia induced (Figures S1E and S1F). Immunofluorescence (IF) staining revealed that PTPMT1 localized at the mitochondria as shown by the co-localizing pattern of PTPMT1 and MitoTracker in the wild-type (MHCC97L-Cas9-EV) subclone (Figure 1F). Also, IF staining further confirmed that PTPMT1 intensity was significantly reduced in the PTPMT1 KO (MHCC97L-Cas9-sgPTPMT1-1 and -sgPTPMT1-2) subclones (Figure 1F). PTPMT1 is an important enzyme for the synthesis of CL. CL binds to all major proteins within the mitochondrial inner membrane (MIM), including solute carriers, ATPase, the ETC complexes, and ADP/ATP carrier. CL is also important for the formation of cristae and allows the assembly of stable complexes of the ETC so that efficient electron transfer and ATP generation could be maintained at the ETC. Transmission electron microscopy (TEM) allows us to closely inspect the cristae (or folding of the MIM) of our HCC subclones. We found that KO of PTPMT1 abrogated the formation of cristae in both normoxic and hypoxic conditions (Figure 2A). Nonyl acridine orange (NAO) specifically stains mitochondria by binding to CL, which is found exclusively in mitochondria with the highest abundance at MIM, allowing us to better visualize the cristae. NAO staining also showed that loss of PTPMT1 disrupted the formation of mitochondrial cristae in HCC cells (Figure 2B). The Seahorse XF Cell Mito Stress Test confirmed that KO of PTPMT1 reduced the oxygen consumption rate (OCR)/mitochondrial activity and respiratory capacity in MHCC97L cells in both normoxic and hypoxic conditions (Figure 2C). JC1 staining indicated that mitochondrial potential was decreased in PTPMT1 KO HCC cells, suggesting that the mitochondria are depolarized with reduced activity (Figures 2D and S1G). Since inhibition of CL impairs the assembly of the ETC complexes, which otherwise trap electrons, we examined the ROS levels in our PTPMT1 KO subclones. CM-H_2DCFDA staining showed that ROS accumulated more dramatically in PTPMT1 KO cells under hypoxia than in normoxia (Figures 2E and S1H). MitoPY1 is a small-molecule fluorescent probe that selectively targets a specific type of ROS, hydrogen peroxide (H_2O_2) produced from mitochondria. MitoPY1 staining further confirmed that loss of PTPMT1 significantly induced mitochondrial ROS accumulation under hypoxia (Figure S1I). Notably, absolute OCRs and relative mitochondrial membrane potentials of hypoxic MHCC97L subclones were significantly lower than their corresponding normoxic MHCC97L subclones (Figures 2C and 2D). This is in line with the conventional understanding that hypoxic cells have decelerated electron transfer and, therefore, reduced mitochondrial activity. Cells rely on PTPMT1 to synthesize CL for proper mitochondrial formation under any circumstances, regardless of the O_2 content. However, ROS- are dramatically induced by hypoxia due to the rapid decline of the electron recipient (O_2). Mitochondrial defect caused by PTPMT1 KO aggravates the electron leakage, as the electrons have no way to be taken up or transferred when ETC complexes could not be assembled in the mitochondrial membrane, leading to further accumulation of oxidative stress. PTPMT1 dephosphorylates PGP to produce PG, which homodimerizes to form CL precursor. Mass spectrometry (MS) analysis was performed to study the change of global lipid profile in PTPMT1 KO subclones under hypoxia. Principal-component analysis (PCA) demonstrated the consistency of the technical repeats in each experimental group (Figures 3A and 3B). Heatmap analysis and volcano plots indicated change of global lipid profile upon PTPMT1 KO in MHCC97L cells under hypoxia, but most of the lipid levels remained statistically unaltered (Figures 3B and S2A). Importantly, the level of phosphatidic acid (PA; lipid upstream of PTPMT1) increased, while the levels of PG and CL (lipids downstream of PTPMT1) decreased in PTPMT1 KO cells, indicative of an impairment of CL synthesis (Figure 3C). A previous study reported that sphingolipid (SL) synthesis was enhanced in murine HCC (Guri et al., 2017). Our MS data demonstrated that the levels of SL lipids, including sphingomyelin (SM), ceramide (Cer), and hexacylceramide (HexCer), were not altered (Figure S2B). Additionally, we performed targeted MS analysis by ultra-performance liquid chromatography coupled with tandem MS (UPLC-MS/MS) to quantify PG and CL in PTPMT1 KO subclones cultured under normoxic or hypoxic conditions. CL

Figure 2. PTPMT1 KO disrupted mitochondrial activity and induced oxidative stress in hypoxic HCC cells

(A) Left: representative TEM images (scale bar: 1 μm) show mitochondria of MHCC97L-Cas9-EV, -sgPTPMT1-1, and -sgPTPMT1-2 subclones cultured in 20% O_2 or 1% O_2 for 48 h. Arrows point to mitochondria. Loss of cristae was found in PTPMT1 KO subclones. Right: quantification of mitochondria with cristae and without cristae. At least 120 mitochondria were counted per experimental group.

(B) Left: representative IF images (scale bar, 2 μm) show mitochondria of MHCC97L-Cas9-EV, -sgPTPMT1-1, and -sgPTPMT1-2 subclones cultured in 20% O_2 or 1% O_2 for 48 h. Insets: magnified images show disruption of cristae in PTPMT1 KO subclones (scale bar, 1 μm). Right: quantification of mitochondria with disrupted cristae and intact cristae. At least 600 mitochondria were counted per experimental group.

(C) Oxygen consumption rates (OCRs) of MHCC97L-Cas9-EV, -sgPTPMT1-1, and -sgPTPMT1-2 subclones cultured in 20% O_2 or 1% O_2 for 48 h were measured with the XFp Cell Mito Stress Test. Quantification of basal respiration, maximal respiration capacity, proton leak, and ATP-linked respiration.

(D and E) In (D), relative mitochondrial potentials were measured by JC-1 staining; in (E), relative intracellular ROS levels were measured by CM-H_2DCFDA staining in MHCC97L-Cas9-EV, -sgPTPMT1-1, and -sgPTPMT1-2 subclones cultured in 20% O_2 or 1% O_2 for 48 h.

Error bars indicate mean ± SEM (n = 3). *p < 0.05; **p < 0.01; ***p < 0.001, Student's t test.

See also Figure S1.

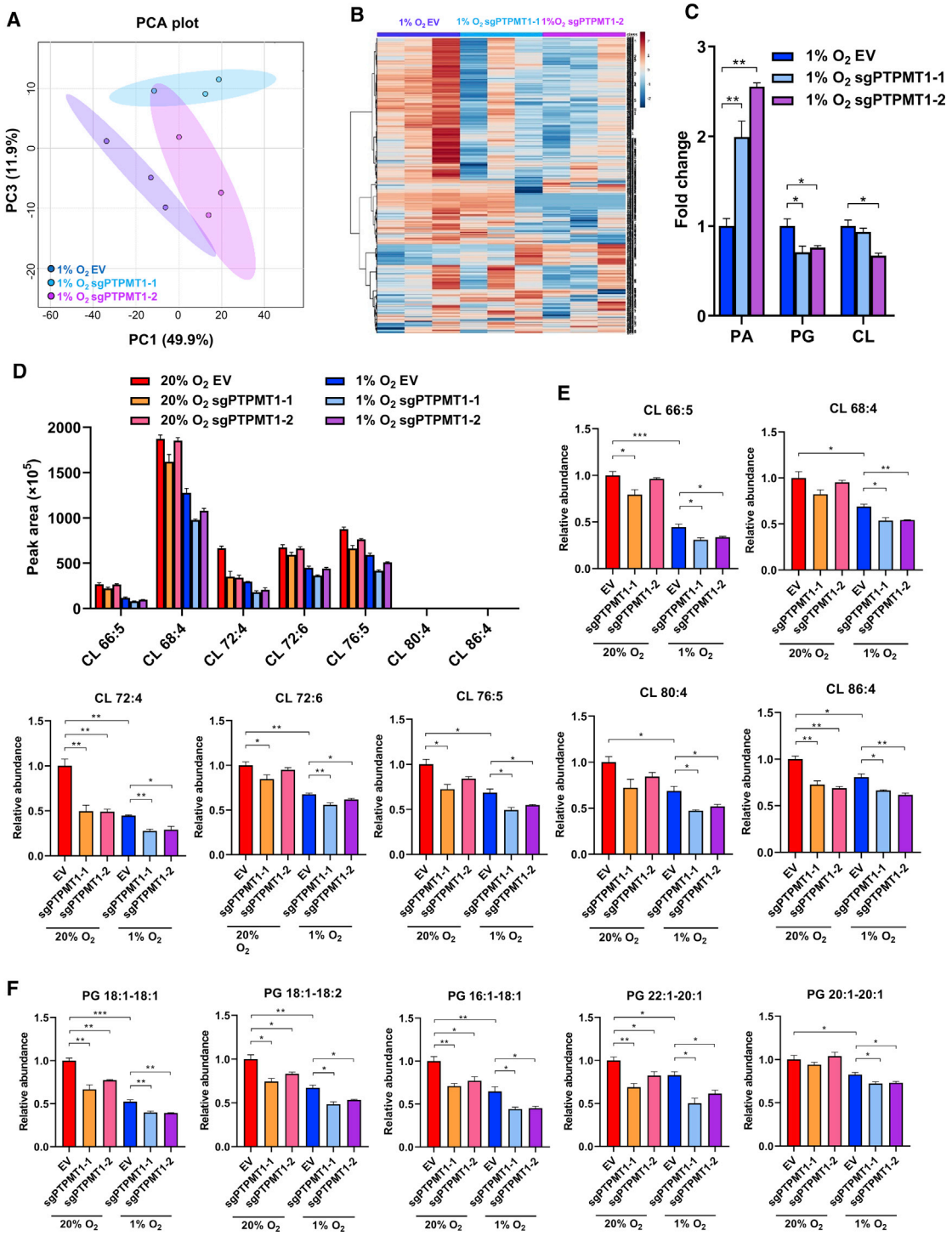

Figure 3. PTPMT1 KO disrupted CL synthesis in hypoxic HCC cells

(A–C) MHCC97L-Cas9-EV, -sgPTPMT1-1, and -sgPTPMT1-2 subclones were cultured in 1% O_2 for 48 h. Metabolites were extracted for untargeted MS analysis. (A) Principal-component analysis (PCA) was performed based on quantity of different lipid species. (B) Heatmap analysis was performed based on quantity of different lipid species. Level of fold change is indicated by the color index: red, positive enrichment; blue, negative enrichment. (C) Fold change of PA, PG, and CL were measured. Values were normalized to 1% O_2 MHCC97L-Cas9-EV.

(legend continued on next page)

68:4 was the most abundant CL species in MHCC97L (Figure 3D). Consistent with lipid profiling data, loss of PTPMT1 led to drastic reduction of CL and PG species, especially under hypoxic conditions (Figure 3E and 3F). A colorimetric-based CL quantification assay also confirmed the MS results (Figure S2C).

PTPMT1 promoted liver cancer growth and progression

Next, we investigated the effects of PTPMT1 on cancer growth *in vitro* and *in vivo*. PTPMT1 KO subclones of MHCC97L proliferated more slowly in general, but the magnitude of growth difference is significantly more prominent in hypoxia relative to normoxia (Figure 4A). Annexin V and phosphatidylinositol (PI) staining demonstrated that KO of PTPMT1 or Ptpmt1 dramatically increased apoptosis in HCC cells, especially in hypoxia (Figures S2D and S2E). We hypothesized that the effects of PTPMT1 depletion were associated with hypoxia-induced ROS. Consistently, exogenous administration of ROS, tert-butyl hydroperoxide (tBHP), significantly induced more extensive apoptosis of PTPMT1 KO subclones (Figure S2F). We performed orthotopic implantation in which MHCC97L-Cas9-EV, -sgPTPMT1-1, and -sgPTPMT1-2 subclones were inoculated into the livers of nude mice. Primary tumors formed by PTPMT1 KO subclones were drastically smaller (Figures 4B and 4C). Histological analysis confirmed that PTPMT1 KO tumors were also less aggressive, with more regular growth fronts and higher degrees of encapsulation (Figure S3A; Table S1). The tendency for lung metastasis was also reduced in PTMPT1 KO subclones (Figure 4D). We also generated a mouse HCC model in immune-competent mice by hydrodynamic tail-vein injection (HDTVi). In HDTVi, we injected a large volume (10% of the body weight) of plasmid mixture into the bloodstream of the mice in 6–8 s. This created high pressure, causing temporary cardiac congestion that back-flushed the plasmids into the livers and resulted in forcible plasmid uptake in hepatocytes. We showed that HDTVi-mediated liver-specific KO of the tumor suppressor gene p53 by CRISPR-Cas9 system and overexpression (OE) of the oncogene c-Myc by the Sleeping Beauty (SB) transposon system consistently induced mouse HCC formation. We further linked an additional sgRNA to target mouse Ptpmt1 to generate Ptpmt1 somatic KO in the liver with p53 KO and c-Myc OE background. Immunohistochemistry (IHC) further confirmed the KO efficiency of Ptpmt1 in mouse livers (Figure 4E). KO of Ptpmt1 significantly reduced tumor volume and tumor weights and yielded less pathologically aggressive tumors (Figures 4F and 4G; Table S2), suggesting that PTPMT1 is indispensable for HCC tumorigenicity.

PTPMT1 inhibitor suppressed growth of liver cancer and other solid cancers *in vivo*

From an *in vitro* small-molecule drug library screening study, alexidine dihydrochloride (AD), a biguanide compound, was identified as a PTPMT1 inhibitor (Doughty-Shenton et al., 2010). We hypothesized that hypoxic cancer cells would be more sensitive to PTPMT1 depletion due to ROS accumulation. XTT assay in different HCC cell lines (MHCC97L, Hep3B, Huh7, and HepG2) showed that the growth inhibitory 50 (GI_{50}) values of PTPMT1 inhibitor (AD) were significantly lower in all HCC cell lines in hypoxia than in normoxia (Figure 5A). Annexin V and PI staining demonstrated that AD induced more extensive apoptosis in MHCC97L cells under hypoxic conditions or in combination with tBHP treatment (Figures 5B and S4A). TEM study and IF staining with NAO confirmed that AD extensively disrupted the formation of cristae in MHCC97L cells (Figures 5C and 5D). Similar to KO of PTPMT1, reduction of OCR and mitochondrial membrane potential could be observed in MHCC97L cells treated with AD as demonstrated by the Seahorse XF Cell Mito Stress Test and JC1 staining, respectively (Figures 5E and 5F). AD dramatically increased a greater amount of ROS in hypoxic MHCC97L cells (Figures 5G and S4B). AD has consistent effects on ROS induction in hypoxic cell lines of different cancer types, including ovarian cancer (ES-2), colorectal cancer (HCT116), breast cancer (MDA-MB-231), pancreatic cancer (MIA Paca-2), and prostate cancer (PC3) (Figures S4C–S4G). By XTT assay in MHCC97L cells, we demonstrated that AD-mediated repression of cell viability could be rescued by two different antioxidants, N-acetyl-cysteine (NAC) and reduced glutathione (GSH), under hypoxic conditions (Figure 6A). We further performed lipidomics analysis and revealed that AD induced change of the global lipid profile in MHCC97L cells under hypoxic conditions (Figures S4H–S4J). AD treatment significantly reduced PG and CL levels in hypoxic HCC cells (Figure S4K). AD did not affect Cer but slightly reduced the levels of SM and HexCer (Figure S4L). We speculated that AD might affect some other molecular targets or cause cell death, leading to a slight discrepancy in the levels of some metabolites from PTPMT1 KO. However, the trends for the key metabolites are consistent in the two lipodomics. Consistently, targeted MS analysis showed that CL 66:4 was the major CL species (Figure 6B). Targeted MS confirmed that AD substantially diminished the levels of CL and PG in MHCC97L cells, especially under hypoxia (Figures 6C and 6D). Colorimetric-based CL quantification assay confirmed that AD lowered CL level in hypoxic HCC cells (Figure S4M). We speculated that AD disrupts mitochondrial membrane, thereby preventing ETC proteins from being anchored properly at the mitochondrial membrane. HCC cells use NDUFA4 under the high O_2 condition and NDUFA4L2 under the low O_2 condition in complex I of ETC to optimize the speed of electron transfer to balance ATP and ROS production at ETC (Lai et al., 2016). Interestingly, western blotting showed that AD drastically reduced the levels of NDUFA4 and NDUFA4L2 under normoxic and hypoxic conditions, respectively, in the mitochondrial extract (Figure S4N), suggesting that AD perturbs the ETC chain formation. To extend our investigation *in vivo*, we used three mouse HCC models to evaluate the efficiency of AD

(D–F) MHCC97L-Cas9-EV, -sgPTPMT1-1, and -sgPTPMT1-2 subclones were cultured in 20% O_2 or 1% O_2 for 48 h. Metabolites were extracted for targeted MS analysis. (D) Absolute abundance and (E) relative abundance of CL were detected in PTPMT1 KO subclones. (F) Relative abundance of PG was detected in PTPMT1 KO subclones. Values were normalized to 20% O_2 MHCC97L-Cas9-EV.

Error bars indicate mean ± SEM (n = 3). *p < 0.05; **p < 0.01; ***p < 0.001, Student's t test.

See also Figure S2.

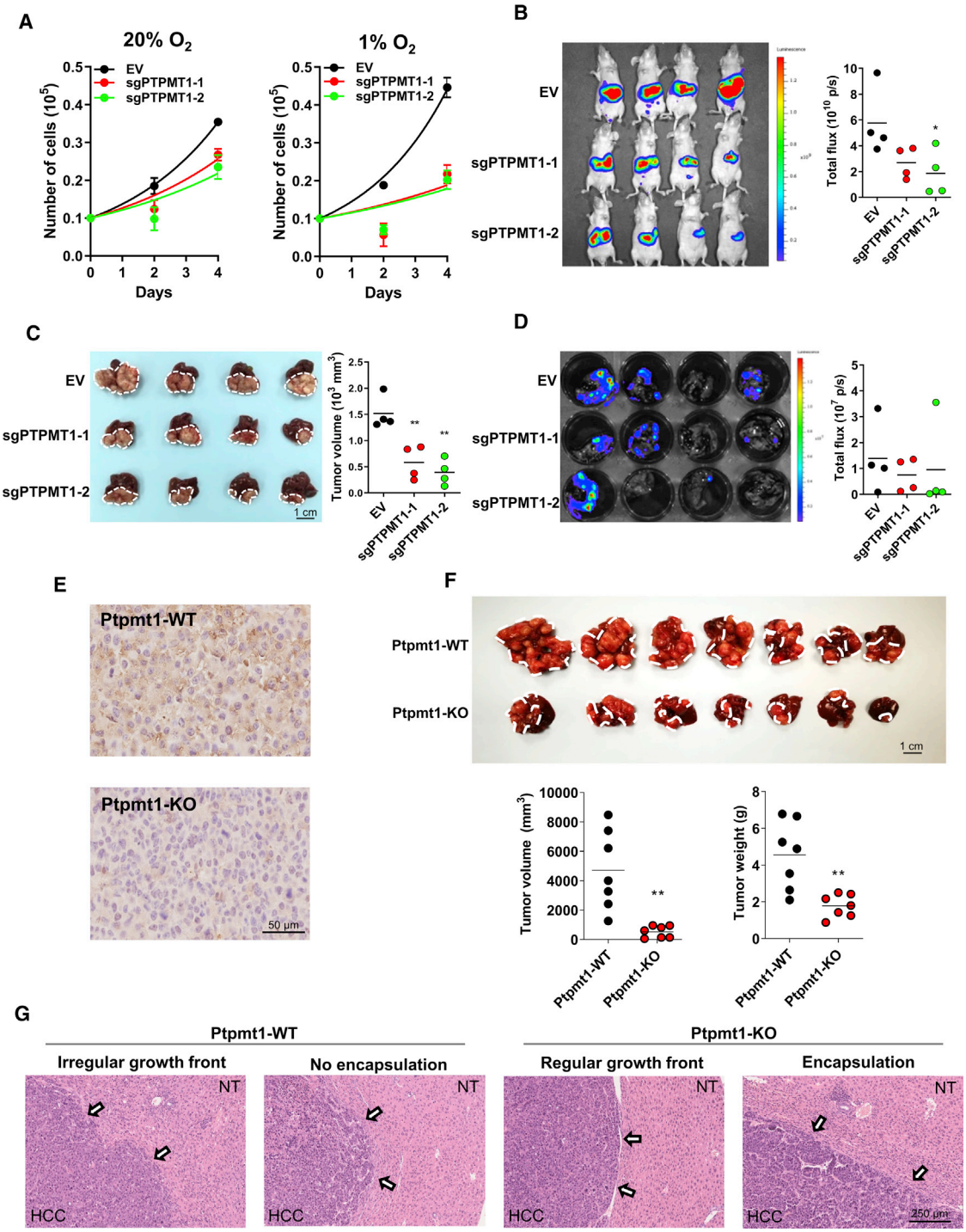

Figure 4. PTPMT1 KO attenuated HCC tumor growth

(A) Cell proliferation rate of MHCC97L-Cas9-EV, -sgPTPMT1-1, and -sgPTPMT1-2 subclones cultured in 20% O_2 or 1% O_2 for 4 days.

(B–D) Luciferase-labeled MHCC97L-Cas9-EV (n = 4), -sgPTPMT1-1 (n = 4), and -sgPTPMT1-2 (n = 4) subclones were orthotopically implanted into the left lobes of the livers of nude mice. (B) Xenogen imaging of mice and quantification of bioluminescence generated from primary HCC tumors. (C) Images of orthotopic xenografts (scale bar, 1 cm) and quantification of tumor volume. (D) Xenogen imaging of lung tissues and quantification of bioluminescence generated from lung metastases.

(E–G) Hydrodynamic tail-vein injection (HDTVi) generated Ptpmt1-wild-type (WT) HCC (n = 7) and Ptpmt1-KO HCC (n = 7) with p53 KO and c-Myc overexpression (OE) background by delivering CRISPR-Cas9 KO and Sleeping Beauty (SB) transposon systems into livers of C57/BL6 mice. (E) IHC images show expression of

(legend continued on next page)

inhibitor as HCC therapeutics. Intraperitoneal (i.p.) injection of 0.5 mg/kg/day of AD treatment significantly suppressed the growth and progression of HCC tumors induced by HDTVi (p53 KO and c-Myc OE) in C57BL/6N, subcutaneous tumors derived from MHCC97L cells in nude mice, and orthotopic tumors derived from luciferase-labeled MHCC97L cells in nude mice, with no adverse effects on the mice as reflected by the unchanged body weights (Figures 6E–6J and S5A–S5C). Histological analysis revealed that AD treatment reduced tumor aggressiveness with more regular tumor growth fronts and higher level of encapsulation in the HDTVi model (Figure S5D; Table S3). AD treatment also blocked lung metastasis derived from orthotopic tumors in mice (Figure 6K). To examine whether this is a generalizable effect in other solid cancers, we evaluated the effects of AD in the growth of ovarian cancer and colorectal cancers. Since ovarian cancer often forms ascites in the peritoneal cavity (Chen et al., 2019), we injected a high-grade serous human ovarian cancer cell line, ES-2, into the peritoneal cavity of female nude mice. Xenogen imaging confirmed that AD significantly suppressed the growth of ovarian cancer in the peritoneal cavity and common metastatic sites of ovarian cancer, including pancreas and intestines (Figures S5E–S5G). There was no significant effect on the body weights of animals (Figure S5H). Similarly, AD significantly suppressed subcutaneous tumors derived from a human colorectal cancer cell line, HCT116, in nude mice (Figure S5I). AD has no adverse effect on animals during the course of experiments, as reflected by the unchanged body weights (Figure S5J).

PTPMT1 OE in human cancers

To understand the clinical relevance of PTPMT1 in human cancers, we investigated the mRNA and protein expression levels of PTPMT1 in human HCC. Quantitative real-time PCR showed that PTPMT1 mRNA was significantly overexpressed in our cohort (QMH-HKU) of HCC tissues relative to the non-tumorous liver (NT) tissues (Figure 7A). 71.67% (43/60) of HCC patients showed at least 1-fold induction of PTPMT1 expression in their HCC tissues (Figure 7A). IHC staining confirmed its OE at the protein level (Figure 7B). The Cancer Genome Atlas (TCGA) database of another cohort of HCC patients further echoed our data that PTPMT1 OE was frequently found in human HCC (Figure 7C). Survival analysis on TCGA data containing more than 300 HCC tissue samples indicated that high PTPMT1 expression in human HCC tissues was significantly associated with poor disease-free survival and overall survival (Figure 7D).

DISCUSSION

Genome-wide CRISPR-Cas9 KO library screening has enabled us to identify the important roles of PTPMT1 in hypoxic adaptation in cancer. PTPMT1 is an important enzyme for the synthesis of CL, an important component of the MIM. Proper CL synthesis is crucial to assembly of ETC complexes, which mediate electron transfer at the ETC. In the presence of O_2, the final electron recipient in the ETC, the electron is transferred efficiently. When O_2 declines, electron transfer becomes inefficient, causing electron leakage and ROS accumulation. HIF-1 allows hypoxic cancer cells to decelerate electron transfer and prevent excessive ROS accumulation by switching on a less active subunit in complex I (NDUFA4L2) and complex IV (COX4-2) (Fukuda et al., 2007; Lai et al., 2016; Tello et al., 2011). Although the ETC activity is lowered by HIF-1, our study highlights that ETC has to be intact, otherwise electrons have nowhere to be transferred, further aggravating ROS accumulation and causing cell death in hypoxia. Therefore, KO of PTPMT1 disabled the assembly of ETC complex through inhibition of CL synthesis and increased ROS excessively in hypoxia.

The most common approaches to identify hypoxia-regulated genes include gene expression microarray, transcriptome sequencing, chromatin immunoprecipitation (ChIP)-chip, and ChIP sequencing. These high-throughput approaches have their unique strengths and limitations. These techniques favor the identification of hypoxia-induced and HIF-target genes that might confer more aggressive cancer traits. However, these techniques missed the genes that are not induced by hypoxia but are essential in the survival of hypoxia. Genes upstream of HIFs are also omitted. In an attempt to study the molecular biology of hypoxic cancer cells from another angle, we conducted forward functional genetic screening by the genome-wide CRISPR-Cas9 KO library to identify genes important for adaptation and survival in hypoxia that the field has neglected. Our screening revealed that PTPMT1, an enzyme crucial to CL synthesis, was one of the most important genes conferring hypoxic cancer cell survival advantages. CL constitutes 20% of the total lipid of MIM and 3% of the total lipid of the mitochondrial outer membrane (MOM). CL is made up of a glycerol head and four acyl chains and is synthesized in the MIM by a series of metabolic enzymes, including TAMM41, PGS, PTPMT1, and Tafazzin (TAZ) (Claypool and Koehler, 2012). CL is important for the formation of cristae and allows the assembly of stable complexes of the ETC. Intact cristae or ETC consumes the electrons and limits excessive flow of electrons through the ETC, thereby restricting ROS production. CL, indeed, plays crucial roles in human physiology. Mutations in the TAZ gene causes CL abnormalities, resulting in Barth syndrome (BTHS). The mitochondria of BTHS patients could not maintain mitochondrial membrane potential with reduced mitochondrial activity (Xu et al., 2005), similar to our observation in the reduction of mitochondrial membrane potential and OCR in our PTPMT1 KO HCC cells. The CL of BTHS patients, unlike normal CL, is structurally variable (Acehan et al., 2007). The BTHS lymphoblast displayed reduced cristae with improper alignment and uneven distribution (Acehan et al.,

Ptpmt1 in the tumors (scale bar, 50 μm). (F) Images of tumors harvested at 36 days post-injection. Tumor volumes and weights were recorded. (G) Representative H&E staining images show growth fronts and tumor encapsulation (indicated by arrows) from tumors derived from HDTVi (scale bar, 250 μm). Ptpmt1-wild-type (WT) HCC tumors (n = 7) show more aggressive phenotypes with irregular tumor growth front and absence of tumor encapsulation, while Ptpmt1-KO HCC tumors (n = 7) show more regular growth front and presence of encapsulation at the boundary of HCC and non-tumoral (NT) tissue.
Data are presented as means. *$p < 0.05$; **$p < 0.01$, Student's t test.
See also Figures S2 and S3 and Tables S1 and S2.

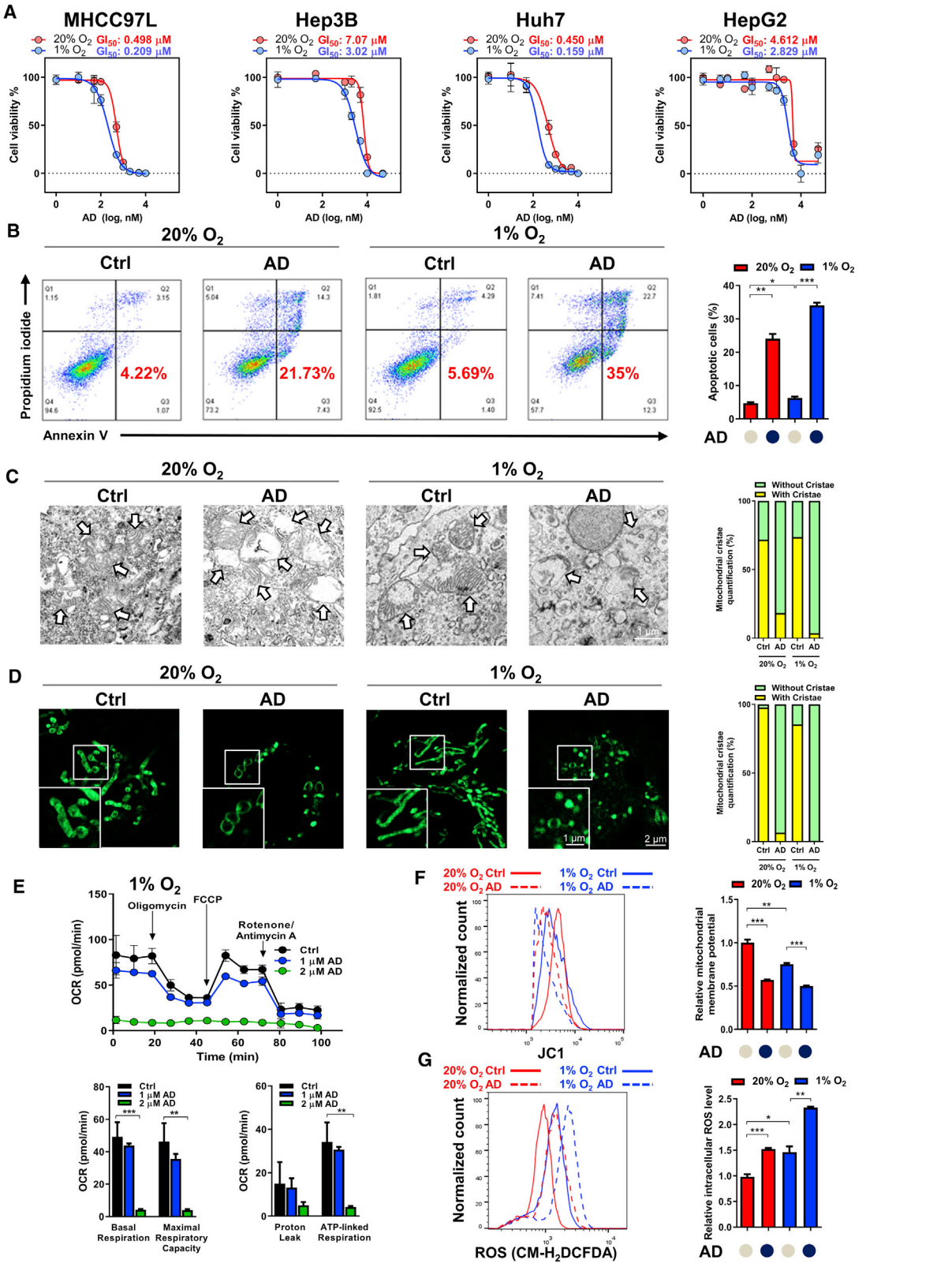

(legend on next page)

2007), similar to what we found in PTPMT1 KO HCC cells. Recently, TAZ was identified in the CRISPR-Cas9 KO library screening as a crucial gene for the stemness maintenance in acute myeloid leukemia cells (Seneviratne et al., 2019), echoing our present study about the relevance of CL synthesis in cancer development. Apart from PTPMT1, which we comprehensively characterized, we found that PGS1, an enzyme directly upstream of PTPMT1, is also important for hypoxic survival of HCC cells (data not shown).

Notably, PTPMT1 is also important to normal cells. Embryonic stem cells (ESCs) and mouse embryonic fibroblasts (MEFs) from PTPMT1 KO mice had lower complex I activity, respiratory rate, and proliferation rate (Shen et al., 2011; Zhang et al., 2011). Hematopoietic-cell-specific PTPMT1 KO impaired hematopoietic stem cell (HSC) differentiation, leading to HSC expansion and embryonic lethality (Yu et al., 2013). Information of PTPMT1 in cancer context is scarce. An early study showed that PTPMT1 in an insulinoma (malignancy of pancreatic β cells) cell line markedly affected the phosphorylation profiles of mitochondrial proteins. PTPMT1 also augmented insulin generation in insulinoma, causing hypoglycemia in patients (Pagliarini et al., 2005). Interestingly, it was reported that PTPMT1 could dephosphorylate and inactivate succinate dehydrogenase (SDHA) in complex II of the ETC in β cells, thereby controlling the ETC metabolic flux (Nath et al., 2015). Our study mainly focused on the roles of PTPMT1 in the dephosphorylation of CL intermediate. Whether PTPMT1's effect on protein dephosphorylation is associated with hypoxic adaptation is unknown at the moment. We, however, believe that PTPMT1's role on CL synthesis creates more direct and immediate survival advantages due to the rapid increase of ROS during hypoxia.

In addition to CL synthesis, we found that some top-ranked genes might have interesting biological implications in hypoxic survival, such as NAE1 (rank #5), SOD2 (rank #8), and TXN (rank #25). NAE1 has been reported to neddylate HIF-1α by transferring NEDD8 to the PAS-B domain of HIF-1α to stabilize HIF-1α (Ryu et al., 2011). Knockdown of NAE1 in MHCC97L cells should theoretically lead to degradation of HIF-1α and induce HCC cell death under hypoxia. SOD and TXN are important players in the antioxidant system. We surmised that hypoxic cells have higher reliance on antioxidant genes, as hypoxia induced oxidative stress due to electron leakage at the ETC. SOD2 is localized at the mitochondrial matrix, and it specifically neutralizes mitochondrial ROS generated from ETC at MIM (Weisiger and Fridovich, 1973). Interestingly, we found that OE of SOD2 in PTPMT1 KO HCC subclones could rescue cell viability (data not shown), further suggesting that PTPMT1 induced cell death via mitochondrial ROS induction. Neddylation of HIF-1α is a less characterized mechanism as compared to other post-translational modifications such as ubiquitination (Ryu et al., 2011). Exemplified by NAE1, our library screening has spotlighted some previously underappreciated mechanisms related to the regulation of HIFs. More mechanistic studies should be focused on how neddylation contributes to hypoxic adaptation and cancer development in the near future. In addition, our library screening has revealed an exhaustive list of genes that are crucial to the survival of hypoxic cancer cells that are valuable to be further investigated by the field.

Hypoxia is irrefutably important to cancer development. HIFs are the transcription factors that mediate almost all biological steps in cancer development and progression. An elegant drug library screening has identified digoxin as an effective HIF-1 inhibitor with potent anti-cancer effects (Samanta et al., 2014; Schito et al., 2012; Wong et al., 2012; Zhang et al., 2012). It was shown extensively that digoxin efficiently suppressed HIF-1-mediated events and cancer development (Samanta et al., 2014; Schito et al., 2012; Wong et al., 2012; Zhang et al., 2012). Digoxin is currently under clinical trial for the treatment of pancreatic cancer as combined therapy with FOLFIRINOX (ClinicalTrials.gov: NCT04141995). Multiple clinical trials on a specific HIF-2α inhibitor (MK-682, previously called PT2977) are underway for the treatment of renal cell carcinoma and advanced solid cancers (ClinicalTrials.gov: NCT03634540 and NCT02974738). While translational emphasis is placed on HIFs, it is also important to identify drugs that target hypoxic cancer cells through HIF-independent mechanisms. AD is a small-molecule inhibitor and a biguanide compound with high activity against PTPMT1 (Doughty-Shenton et al., 2010). Although a more specific PTPMT1 inhibitor is awaited, we used AD as proof of concept to demonstrate the translational implications of our library

Figure 5. Pharmacological inhibition of PTPMT1 reduced mitochondrial activity and induced oxidative stress in hypoxic HCC cells

(A) GI_{50} values of AD in different HCC cell lines, including MHCC97L, Hep3B, Huh7, and HepG2 cultured in 20% O_2 or 1% O_2.

(B) Annexin V and PI staining of MHCC97L cells treated with control (Ctrl; gray circles) or 5 μM AD (navy circles) cultured in 20% O_2 or 1% O_2 for 24 h.

(C) Left: representative TEM images (scale bar, 1 μm) show mitochondria of MHCC97L cells treated with Ctrl (gray circles) or 1 μM AD (navy circles) cultured in 20% O_2 or 1% O_2 for 48 h. Arrows point to mitochondria. Loss of cristae was found in cells treated with AD. Right: quantification of mitochondria with cristae and without cristae. At least 50 mitochondria were counted per experimental group.

(D) Left: representative IF images (scale bar, 2 μm) show mitochondria of MHCC97L cells treated with Ctrl (gray circles) or 1 μM AD (navy circles) cultured in 20% O_2 or 1% O_2 for 48 h. Insets: magnified images show loss of cristae in cells treated with AD (scale bar, 1 μm). Right: quantification of mitochondria with cristae and without cristae. At least 500 mitochondria were counted per experimental group.

(E) Oxygen consumption rates (OCRs) in MHCC97L cells treated with Ctrl, 1 μM AD, and 2 μM AD cultured in 20% O_2 or 1% O_2 for 48 h were measured with the XFp Cell Mito Stress Test. Basal respiration, maximal respiration capacity, proton leak, and ATP-linked respiration were calculated.

(F) JC-1 staining followed by flow cytometry indicates the mitochondrial potential of MHCC97L cells treated with Ctrl or 1 μM AD cultured in 20% O_2 or 1% O_2 for 48 h.

(G) CM-H_2DCFDA staining followed by flow cytometry indicates the ROS levels in MHCC97L cells treated with Ctrl (gray circles) or 1 μM AD (navy circles) cultured in 20% O_2 or 1% O_2 for 48 h.

Error bars indicate mean ± SEM (n = 3). *p < 0.05; **p < 0.01; ***p < 0.001, Student's t test.

See also Figure S4.

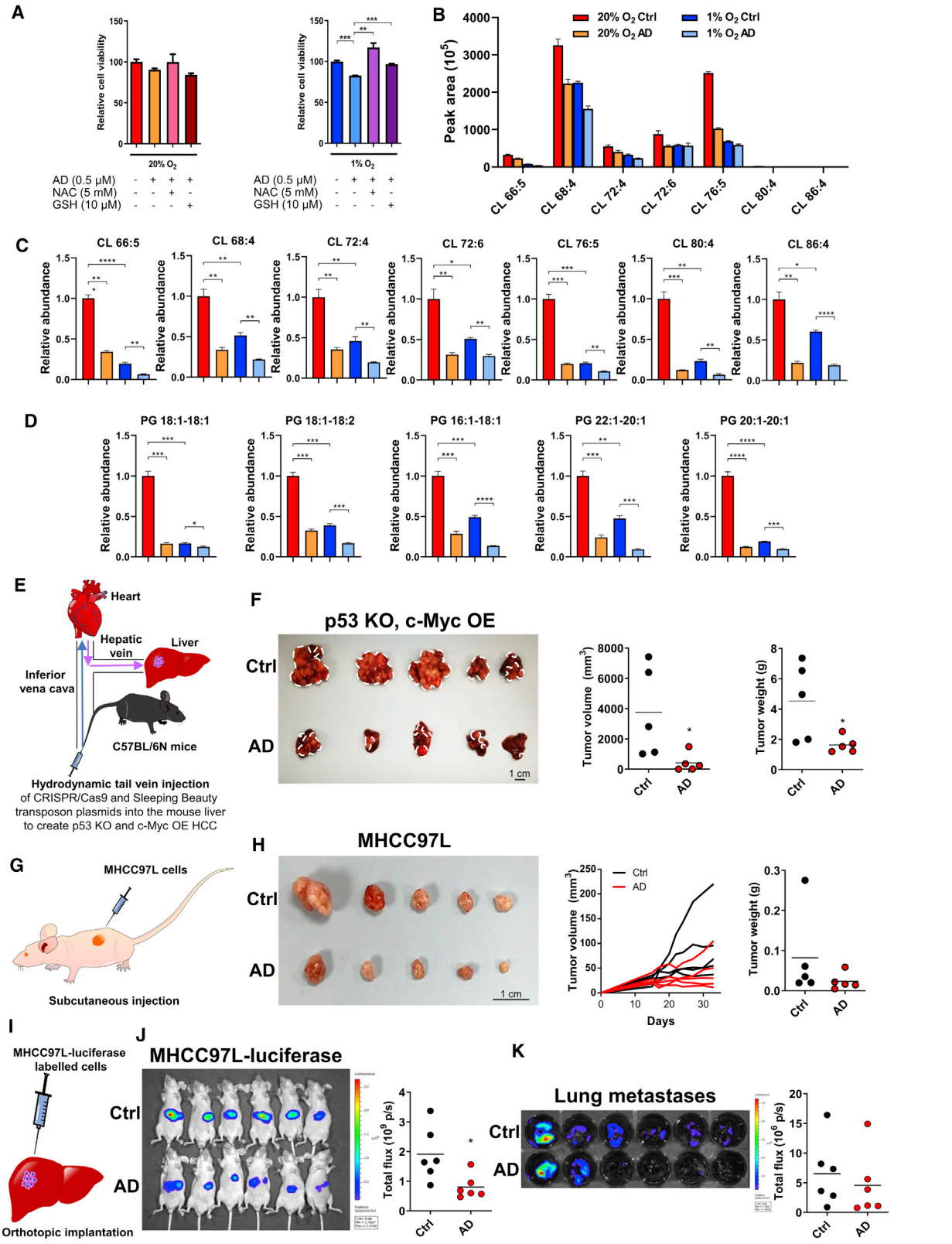

(legend on next page)

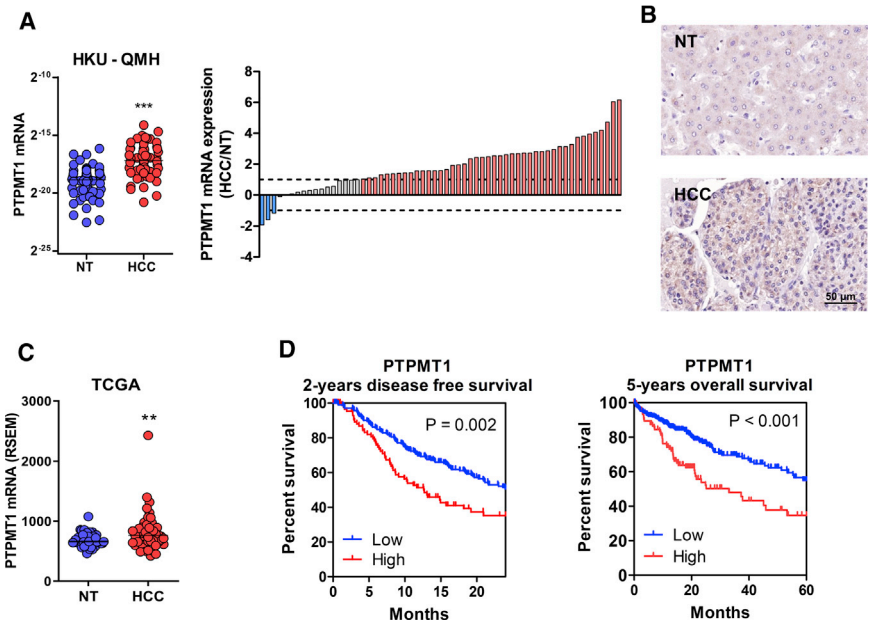

Figure 7. PTPMT1 is overexpressed in HCC patients

(A) PTPMT1 mRNA expression in 60 cases of human HCC and non-tumorous liver (NT) tissues was determined by quantitative real-time PCR in the QMH-HKU cohort. Data were calculated based on the formula: $2^{-(CT\ of\ PTPMT1\ -\ CT\ of\ 18S)}$. Waterfall plot shows 71.67% (43/60) of HCC patients from the QMH-HKU cohort with at least 1-fold PTPMT1 OE in HCC tissues.

(B) IHC staining shows PTPMT1 overexpression in human HCC tissues at the protein level.

(C) PTPMT1 mRNA expression in 49 cases of human HCC and non-tumorous liver (NT) tissue from TCGA database (RSEM, RNA-Seq by Expectation Maximization).

(D) High expression of PTPMT1 in human HCC was significantly associated with poor overall and disease-free survival of the patients. PTPMT1 expression and survival data were retrieved from TCGA dataset.

screening. As CL is an integral component of the MIM, which is crucial to OXPHOS and mitochondrial functions, PTPMT1 inhibitor can also inhibit growth of normoxic cancer cells. However, since rapid accumulation of ROS can be detrimental to hypoxic cancer cells, our XTT assay demonstrated that hypoxic HCC cells are more sensitive to AD treatment than normoxic HCC cells. A study showed that AD inhibited the viability of head and neck cancer cell lines at 1.8–2.6 μM, while untransformed cells such as fibroblasts were much more resistant to AD, with an half maximal effective concentration (EC_{50}) value about 10 times higher than that of cancer cell lines (Yip et al., 2006). In addition to HCC, our study also shows that AD suppressed the progression of other cancer types, including ovarian cancer and colorectal cancer, at doses that do not affect the body weights of the animals. Our study highlights the idea that inhibitors targeting hypoxic cancer cells are not limited to HIF inhibitors. Apart from PTPMT1, our study has provided a comprehensive and unbiased list of molecular targets that could be harnessed in cancer therapies, especially for cancers that are highly hypoxic.

STAR★METHODS

Detailed methods are provided in the online version of this paper and include the following:

- KEY RESOURCES TABLE
- RESOURCE AVAILABILITY
  - Lead contact
  - Materials availability
  - Data and code availability
- EXPERIMENTAL MODEL AND SUBJECT DETAILS
  - Cell culture

Figure 6. PTPMT1 inhibition disrupted CL synthesis pathway and suppressed HCC growth

(A) XTT assay of MHCC97L cells treated in the presence (+) or absence (–) of 0.5 μM AD, 5 mM NAC, and 10 μM GSH of MHCC97L cultured in 20% O_2 or 1% O_2 for 96 h.

(B–D) MHCC97L cells treated with control (Ctrl) or 2 μM AD were cultured in 20% O_2 or 1% O_2 for 48 h. Metabolites were extracted for targeted MS analysis. (B) Absolute abundance of CL, (C) relative abundance of CL, and (D) PG were measured. Values were normalized to 20% O_2 Ctrl.

(E) Schematic diagram of hydrodynamic tail-vein injection (HDTVi) model. C57BL/6N mice were injected with CRISPR-Cas9-KO plasmid together with Sleeping Beauty (SB) transposon system plasmid to knock out p53 and overexpress c-Myc to induce HCC. Mice were administered with vehicle Ctrl (n = 5) or 0.5 mg/kg/day AD (n = 5) by intraperitoneal (i.p.) injection.

(F) Images of tumors from Ctrl- and AD-treated animals (scale bar, 1 cm). Quantification of tumor volume and tumor weight.

(G) Schematic diagram of subcutaneous HCC model. MHCC97L cells were injected into nude mice subcutaneously. Mice were administered with Ctrl (n = 5) or 0.5 mg/kg/day AD (n = 5) by i.p. injection.

(H) Image of tumors from Ctrl- and AD-treated animals (scale bar, 1 cm). Quantification of tumor volume and tumor weight.

(I) Schematic diagram of orthotopic HCC model. Luciferase-labeled MHCC97L cells were injected into left lobes of the livers of nude mice. Mice were administered with Ctrl (n = 6) or 0.5 mg/kg/day AD (n = 6) by i.p. injection.

(J) Xenogen imaging of mice and quantification of bioluminescence generated from primary HCC tumors.

(K) Xenogen imaging of lung tissues and quantification of bioluminescence generated from lung metastases.

Data are presented as means. Error bars indicate mean ± SEM (n = 3). *p < 0.05; **p < 0.01; ***p < 0.001; ****p < 0.0001, Student's t test.

See also Figures S4 and S5 and Table S3.

SUPPLEMENTAL INFORMATION

Supplemental Information can be found online at https://doi.org/10.1016/j.celrep.2020.108676.

ACKNOWLEDGMENTS

The authors thank the Imaging and Flow Cytometry Core, as well as the Proteomics and Metabolomics Core, from the Centre for PanorOmic Sciences (CPOS), HKU Li Ka Shing Faculty of Medicine, for support in flow cytometry analyses, Xenogen *in vivo* imaging, IF imaging, and targeted MS measurements. We also thank the Centre for Comparative Medicine Research (CCMR), HKU Li Ka Shing Faculty of Medicine, for their support in our animal experiments. We are grateful for the assistance from the Electron Microscope Unit, The University of Hong Kong, for TEM imaging. The study was funded by the Research Grant Council General Research Fund (Project #17101119), Research Grant Council-Theme Based Research Fund (T12-704/16-R), Croucher Innovation Award, and HKU Outstanding Young Researcher Award, HKU, HKSAR.

AUTHOR CONTRIBUTIONS

M.H.-R.B., A.P.-W.T., and L.W. performed hypoxic CRISPR-Cas9 KO library screening. L.W. analyzed the CRISPR-Cas9 KO library screening data. C.Y. performed lipidomics and data analysis. C.Y.-S.C. advised on targeted lipidomics. M.H.-R.B., D.L., M.S.Z., D.K.-C.C., C.C.G., V.W.-H.Y., C.-T.L., W.-C.C., N.N.-Q.C., B.P.-Y.W., C.Y.-K.C., and C.C.-L.W. performed *in vitro* and/or *in vivo* experiments and/or analyzed data. I.O.-L.N. provided clinical samples of human HCC. C.-M.W. and C.C.-L.W. supervised the project. All authors discussed and commented on the manuscript.

DECLARATION OF INTERESTS

The authors declare no competing interests.

Received: March 24, 2020
Revised: November 11, 2020
Accepted: December 30, 2020
Published: January 26, 2021

REFERENCES

Acehan, D., Xu, Y., Stokes, D.L., and Schlame, M. (2007). Comparison of lymphoblast mitochondria from normal subjects and patients with Barth syndrome using electron microscopic tomography. Lab. Invest. *87*, 40–48.

Barrangou, R., Fremaux, C., Deveau, H., Richards, M., Boyaval, P., Moineau, S., Romero, D.A., and Horvath, P. (2007). CRISPR provides acquired resistance against viruses in prokaryotes. Science *315*, 1709–1712.

Bruix, J., Qin, S., Merle, P., Granito, A., Huang, Y.H., Bodoky, G., Pracht, M., Yokosuka, O., Rosmorduc, O., Breder, V., et al.; RESORCE Investigators (2017). Regorafenib for patients with hepatocellular carcinoma who progressed on sorafenib treatment (RESORCE): a randomised, double-blind, placebo-controlled, phase 3 trial. Lancet *389*, 56–66.

Chen, R.R., Yung, M.M.H., Xuan, Y., Zhan, S., Leung, L.L., Liang, R.R., Leung, T.H.Y., Yang, H., Xu, D., Sharma, R., et al. (2019). Targeting of lipid metabolism with a metabolic inhibitor cocktail eradicates peritoneal metastases in ovarian cancer cells. Commun. Biol. *2*, 281.

Claypool, S.M., and Koehler, C.M. (2012). The complexity of cardiolipin in health and disease. Trends Biochem. Sci. *37*, 32–41.

Doughty-Shenton, D., Joseph, J.D., Zhang, J., Pagliarini, D.J., Kim, Y., Lu, D., Dixon, J.E., and Casey, P.J. (2010). Pharmacological targeting of the mitochondrial phosphatase PTPMT1. J. Pharmacol. Exp. Ther. *333*, 584–592.

Ejsing, C.S., Sampaio, J.L., Surendranath, V., Duchoslav, E., Ekroos, K., Klemm, R.W., Simons, K., and Shevchenko, A. (2009). Global analysis of the yeast lipidome by quantitative shotgun mass spectrometry. Proc. Natl. Acad. Sci. USA *106*, 2136–2141.

El-Khoueiry, A.B., Sangro, B., Yau, T., Crocenzi, T.S., Kudo, M., Hsu, C., Kim, T.Y., Choo, S.P., Trojan, J., Welling, T.H.R., et al. (2017). Nivolumab in patients with advanced hepatocellular carcinoma (CheckMate 040): an open-label, non-comparative, phase 1/2 dose escalation and expansion trial. Lancet *389*, 2492–2502.

Epstein, A.C., Gleadle, J.M., McNeill, L.A., Hewitson, K.S., O'Rourke, J., Mole, D.R., Mukherji, M., Metzen, E., Wilson, M.I., Dhanda, A., et al. (2001). C. elegans EGL-9 and mammalian homologs define a family of dioxygenases that regulate HIF by prolyl hydroxylation. Cell *107*, 43–54.

Fukuda, R., Zhang, H., Kim, J.W., Shimoda, L., Dang, C.V., and Semenza, G.L. (2007). HIF-1 regulates cytochrome oxidase subunits to optimize efficiency of respiration in hypoxic cells. Cell *129*, 111–122.

Guri, Y., Colombi, M., Dazert, E., Hindupur, S.K., Roszik, J., Moes, S., Jenoe, P., Heim, M.H., Riezman, I., Riezman, H., and Hall, M.N. (2017). mTORC2 Promotes Tumorigenesis via Lipid Synthesis. Cancer Cell *32*, 807–823.e12.

Herzog, R., Schwudke, D., Schuhmann, K., Sampaio, J.L., Bornstein, S.R., Schroeder, M., and Shevchenko, A. (2011). A novel informatics concept for high-throughput shotgun lipidomics based on the molecular fragmentation query language. Genome Biol. *12*, R8.

Herzog, R., Schuhmann, K., Schwudke, D., Sampaio, J.L., Bornstein, S.R., Schroeder, M., and Shevchenko, A. (2012). LipidXplorer: a software for consensual cross-platform lipidomics. PLoS ONE *7*, e29851.

Kaelin, W.G., Jr., and Ratcliffe, P.J. (2008). Oxygen sensing by metazoans: the central role of the HIF hydroxylase pathway. Mol. Cell *30*, 393–402.

Lai, R.K., Xu, I.M., Chiu, D.K., Tse, A.P., Wei, L.L., Law, C.T., Lee, D., Wong, C.M., Wong, M.P., Ng, I.O., and Wong, C.C. (2016). NDUFA4L2 Fine-tunes Oxidative Stress in Hepatocellular Carcinoma. Clin. Cancer Res. *22*, 3105–3117.

Li, W., Xu, H., Xiao, T., Cong, L., Love, M.I., Zhang, F., Irizarry, R.A., Liu, J.S., Brown, M., and Liu, X.S. (2014). MAGeCK enables robust identification of essential genes from genome-scale CRISPR/Cas9 knockout screens. Genome Biol. *15*, 554.

Llovet, J.M., Ricci, S., Mazzaferro, V., Hilgard, P., Gane, E., Blanc, J.F., de Oliveira, A.C., Santoro, A., Raoul, J.L., Forner, A., et al.; SHARP Investigators Study Group (2008). Sorafenib in advanced hepatocellular carcinoma. N. Engl. J. Med. *359*, 378–390.

Nath, A.K., Ryu, J.H., Jin, Y.N., Roberts, L.D., Dejam, A., Gerszten, R.E., and Peterson, R.T. (2015). PTPMT1 Inhibition Lowers Glucose through Succinate Dehydrogenase Phosphorylation. Cell Rep. *10*, 694–701.

Pagliarini, D.J., Wiley, S.E., Kimple, M.E., Dixon, J.R., Kelly, P., Worby, C.A., Casey, P.J., and Dixon, J.E. (2005). Involvement of a mitochondrial phosphatase in the regulation of ATP production and insulin secretion in pancreatic beta cells. Mol. Cell *19*, 197–207.

Ryu, J.H., Li, S.H., Park, H.S., Park, J.W., Lee, B., and Chun, Y.S. (2011). Hypoxia-inducible factor α subunit stabilization by NEDD8 conjugation is reactive oxygen species-dependent. J. Biol. Chem. *286*, 6963–6970.

Samanta, D., Gilkes, D.M., Chaturvedi, P., Xiang, L., and Semenza, G.L. (2014). Hypoxia-inducible factors are required for chemotherapy resistance of breast cancer stem cells. Proc. Natl. Acad. Sci. USA *111*, E5429–E5438.

Sampaio, J.L., Gerl, M.J., Klose, C., Ejsing, C.S., Beug, H., Simons, K., and Shevchenko, A. (2011). Membrane lipidome of an epithelial cell line. Proc. Natl. Acad. Sci. USA *108*, 1903–1907.

Sanjana, N.E., Shalem, O., and Zhang, F. (2014). Improved vectors and genome-wide libraries for CRISPR screening. Nat. Methods *11*, 783–784.

Schito, L., Rey, S., Tafani, M., Zhang, H., Wong, C.C., Russo, A., Russo, M.A., and Semenza, G.L. (2012). Hypoxia-inducible factor 1-dependent expression of platelet-derived growth factor B promotes lymphatic metastasis of hypoxic breast cancer cells. Proc. Natl. Acad. Sci. USA *109*, E2707–E2716.

Semenza, G.L. (2012). Hypoxia-inducible factors in physiology and medicine. Cell *148*, 399–408.

Seneviratne, A.K., Xu, M., Aristizabal Henao, J.J., Fajardo, V.A., Hao, Z., Voisin, V., Xu, G.W., Hurren, R., Kim, S., MacLean, N., et al. (2019). The Mitochondrial Transacylase, Tafazzin, Regulates AML Stemness by Modulating Intracellular Levels of Phospholipids. Cell Stem Cell *24*, 1007.

Shalem, O., Sanjana, N.E., and Zhang, F. (2015). High-throughput functional genomics using CRISPR-Cas9. Nat. Rev. Genet. *16*, 299–311.

Shen, J., Liu, X., Yu, W.M., Liu, J., Nibbelink, M.G., Guo, C., Finkel, T., and Qu, C.K. (2011). A critical role of mitochondrial phosphatase Ptpmt1 in embryogenesis reveals a mitochondrial metabolic stress-induced differentiation checkpoint in embryonic stem cells. Mol. Cell. Biol. *31*, 4902–4916.

Tello, D., Balsa, E., Acosta-Iborra, B., Fuertes-Yebra, E., Elorza, A., Ordóñez, Á., Corral-Escariz, M., Soro, I., López-Bernardo, E., Perales-Clemente, E., et al. (2011). Induction of the mitochondrial NDUFA4L2 protein by HIF-1α decreases oxygen consumption by inhibiting Complex I activity. Cell Metab. *14*, 768–779.

Wang, G.L., Jiang, B.H., Rue, E.A., and Semenza, G.L. (1995). Hypoxia-inducible factor 1 is a basic-helix-loop-helix-PAS heterodimer regulated by cellular O2 tension. Proc. Natl. Acad. Sci. USA *92*, 5510–5514.

Wei, L., Lee, D., Law, C.T., Zhang, M.S., Shen, J., Chin, D.W., Zhang, A., Tsang, F.H., Wong, C.L., Ng, I.O., et al. (2019). Genome-wide CRISPR/Cas9 library screening identified PHGDH as a critical driver for Sorafenib resistance in HCC. Nat. Commun. *10*, 4681.

Weisiger, R.A., and Fridovich, I. (1973). Mitochondrial superoxide simutase. Site of synthesis and intramitochondrial localization. J. Biol. Chem. *248*, 4793–4796.

Wong, C.C., Zhang, H., Gilkes, D.M., Chen, J., Wei, H., Chaturvedi, P., Hubbi, M.E., and Semenza, G.L. (2012). Inhibitors of hypoxia-inducible factor 1 block breast cancer metastatic niche formation and lung metastasis. J. Mol. Med. (Berl.) *90*, 803–815.

Xu, Y., Sutachan, J.J., Plesken, H., Kelley, R.I., and Schlame, M. (2005). Characterization of lymphoblast mitochondria from patients with Barth syndrome. Lab. Invest. *85*, 823–830.

Xu, G., Liu, X., Shu, Y., Pillai, J.A., and Xu, Y. (2018). A rapid and sensitive LC-MS/MS method for quantitative analysis of cardiolipin $(18:2)_4$ in human leukocytes and mouse skeletal muscles. J. Pharm. Biomed. Anal. *158*, 386–394.

Yip, K.W., Ito, E., Mao, X., Au, P.Y., Hedley, D.W., Mocanu, J.D., Bastianutto, C., Schimmer, A., and Liu, F.F. (2006). Potential use of alexidine dihydrochloride as an apoptosis-promoting anticancer agent. Mol. Cancer Ther. *5*, 2234–2240.

Yu, W.M., Liu, X., Shen, J., Jovanovic, O., Pohl, E.E., Gerson, S.L., Finkel, T., Broxmeyer, H.E., and Qu, C.K. (2013). Metabolic regulation by the mitochondrial phosphatase PTPMT1 is required for hematopoietic stem cell differentiation. Cell Stem Cell *12*, 62–74.

Zhang, J., Guan, Z., Murphy, A.N., Wiley, S.E., Perkins, G.A., Worby, C.A., Engel, J.L., Heacock, P., Nguyen, O.K., Wang, J.H., et al. (2011). Mitochondrial phosphatase PTPMT1 is essential for cardiolipin biosynthesis. Cell Metab. *13*, 690–700.

Zhang, H., Wong, C.C., Wei, H., Gilkes, D.M., Korangath, P., Chaturvedi, P., Schito, L., Chen, J., Krishnamachary, B., Winnard, P.T., Jr., et al. (2012). HIF-1-dependent expression of angiopoietin-like 4 and L1CAM mediates vascular metastasis of hypoxic breast cancer cells to the lungs. Oncogene *31*, 1757–1770.

Zhou, Y., Zhu, S., Cai, C., Yuan, P., Li, C., Huang, Y., and Wei, W. (2014). High-throughput screening of a CRISPR/Cas9 library for functional genomics in human cells. Nature *509*, 487–491.

STAR★METHODS

KEY RESOURCES TABLE

REAGENT or RESOURCE	SOURCE	IDENTIFIER
Antibodies		
Rabbit anti-PTPMT1	The Human Protein Atlas	Cat#HPA043932; RRID: AB_2678738
Rabbit anti-Ptpmt1	Proteintech	Cat#11493-1-AP; RRID: AB_2237967
Rabbit anti-NDUFA4L2	Abcam	RRID: AB_2313773
Mouse anti- β-actin	Sigma-Aldrich	Cat# A2228: RRID: AB_476697
Chemicals, peptides, and recombinant proteins		
DMEM-HG	Thermo Fisher Scientific	Cat#12100-046
F-12K	ATCC	Cat#30-2004
Fetal bovine serum	GIBCO	Cat#16000069
Penicillin-streptomycin	GIBCO	Cat#15140122
T4 DNA Ligase	Invitrogen	Cat#15224017
lentiCas9-Blast	Sanjana et al., 2014	Cat#52962
pLentiGuide-Puro	Sanjana et al., 2014	Cat#52963
EcoRI	NEB	Cat#R3101S
*Age*I	NEB	Cat#R3552S
*Bsm*BI	NEB	Cat#R0580S
Lipofectamine 2000 Transfection Reagent	Thermo Fisher Scientific	Cat#11668019
Puromycin	Sigma-Aldrich	Cat#58-58-2
Alexidine dihydrochloride	Cayman	Cat#13876
Human GeCKO v2A CRISPR-Cas9 knockout pooled library	Sanjana et al., 2014	Cat#1000000048
NEBNext® High-Fidelity 2X PCR Master Mix	NEB	Cat#M0541L
TRIzol® reagent	Ambion®	Cat#15596018
SYBR Green qPCR Master Mix	Applied Biosystems	Cat#4309155
N-acetyl-L-cysteine (NAC)	Sigma-Aldrich	Cat#616-91-1
L-glutathione reduced (GSH)	Sigma-Aldrich	Cat#70-18-8
PEGE-400	Sigma-Aldrich	Cat#25322-68-3
cOmplete™ protease inhibitor	Roche	Cat#04693116001
PhosSTOP phosphatase inhibitor cocktails	Roche	Cat#4906837001
MitoTracker Red FM	Thermo Fisher Scientific	Cat#M22426
Triton X-100	Sigma-Aldrich	Cat#9002-93-1
DAPI	Abcam	Cat#28718-90-3
5,5′,6,6’-tetrachloro-1,1’,3,3′-tetraethyl-benzimidazolylcarbocyanine chloride	Invitrogen	Cat#T3168
chloromethyl-20,70-dichlorodihydrofluorescein diacetate (CM-H_2DCFDA)	Life Technologies	Cat#C6827
MitoPY1	Tocris Bioscience	Cat#4428
tert-Butyl hydroperoxide (tBHP)	Thermo Fisher Scientific	Cat#AC180340050
3,3′-diaminobenzidine (DAB)	Sigma-Aldrich	Cat#91-95-2
Propidium iodide	Calbiochem	Cat#25535-16-4
CL internal standard mixture 1	Aventi	Cat#LM6003
Critical commercial assays		
GeneAmp Gold RNA PCR Core Kit	Applied Biosystems	Cat# N8080143
XFp Cell Mito Stress Test	Aligent	Cat#103010-100
Mitochondria Isolation Kit	Thermo Fisher Scientific	Cat#89874
Cardiolipin Assay Kit	BioVision	Cat#K944

(*Continued on next page*)

Continued

REAGENT or RESOURCE	SOURCE	IDENTIFIER
Cell Proliferation Kit II (XTT	Roche	Cat#11465015001
Annexin V-FITC Kit	MBL International Corporation	Cat#4700
Deposited Data		
CRISPR library of hypoxia treated HCC	This paper	NCBI: PRJNA673757
Experimental models: cell lines		
MHCC97L	Dr. Z.Y. Yang	RRID: CVCL_4973
Hep3B	ATCC	RRID: CVCL_0326
Huh7	Dr. Hidekazu Nakabayashi	RRID: CVCL_0336
Hep G2	ATCC	RRID: CVCL_0027
Hepa1-6	ATCC	RRID: CVCL_0327
ES-2	ATCC	RRID: CVCL_AX39
HCT116	Prof. Bert Vogelstein	RRID: CVCL_0291
MDA-MB-231	ATCC	RRID: CVCL_0062
MIA PaCa-2	ATCC	RRID: CVCL_0428
PC3	ATCC	RRID: CVCL_0035
Oligonucleotides		
Oligonucleotide for cell line establishment: Table S4	This paper	N/A
Primers for RT-qPCR: Table S5	This paper	N/A
Software and Algorithms		
MAGeCK v0.5.7	Li et al., 2014	N/A
ImageJ	Java	https://imagej.nih.gov/ij/
NDP.view2	Hamamatsu	https://www.hamamatsu.com/us/en/product/type/U12388-01/index.html
Excel 2010	Microsoft	N/A
GraphPad Prism 7.0	GraphPad Software	https://www.graphpad.com/

RESOURCE AVAILABILITY

Lead contact

Further information and requests for resources and reagents should be directed to and will be fulfilled by the Lead Contact, Carmen Chak-Lui Wong (carmencl@pathology.hku.hk).

Materials availability

This study did not generate new unique reagents.

Data and code availability

The accession number for the genome-wide CRISPR-Cas9 library screening in HCC reported in this paper is NCBI: PRJNA673757.

EXPERIMENTAL MODEL AND SUBJECT DETAILS

Cell culture

Human HCC cell lines including MHCC97L, Hep3B, Huh7 and Hep G2, mouse HCC cell line Hepa1-6, human ovarian cancer cell line ES-2, human colorectal cell line HCT116, human breast cancer cell line MDA-MB-231, human pancreatic cancer cell lines MIA PaCa-2 as well as human prostate cancer cell line PC3 were used. MHCC97L was a gift from Dr. Z.Y. Yang (Fudan University of Shanghai). Hep3B, HepG2, Hepa1-6, ES-2, MDA-MB-231, MIA PaCa-2, and PC3 were purchased from the American Type Culture Collect (ATCC). Huh-7 was obtained from Dr. Hidekazu Nakabayashi (Hokkaido University). HCT116 was obtained from Prof. Bert Vogelstein (Johns Hopkins University). MHCC97L, Hep3B, Huh7, HepG2, Hepa1-6, ES-2, HCT116, MDA-MB-231 and MIA PaCa-2 were cultured in Dulbecco's Modified Eagle's Medium-high glucose (DMEM-HG) (Thermo Fisher Scientific). PC3 was maintained in Kaighn's Modification of Ham's F-12 (F-12K) medium. All media were supplemented with 10% fetal bovine serum (FBS) (GIBCO) and 1% penicillin-streptomycin (GIBCO). All cells were cultured in 5% CO_2, 95% air incubator at 37°C. For hypoxic treatment, cells were cultured in 1% O_2, 5% CO_2 in N2 (Linde HKO) in modulator incubator chamber (Billups-Rothenberg) at 37°C for 48 h,

unless specified. All cell lines have been authenticated by AuthentiFiler PCR Amplification Kit (Applied Biosystems) and are routinely tested as mycoplasma free.

Establishment of knockdown, knockout, and overexpression cancer cell lines

Table S4 MHCC97L-Cas9 and Hepa1-6-Cas9 stable cells were established by transfecting cells with lentiCas9-Blast vector (Addgene) (Sanjana et al., 2014; Wei et al., 2019). MHCC97L-Cas9 was used to generate PTPMT1 KO cells, and Hepa1-6-Cas9 were used to generate Ptpmt1 knockout cells with pLentiGuide-Puro vector (Addgene) (Sanjana et al., 2014). pLentiGuide-Puro vector encompassing single-guide RNAs (sgRNAs) targeting PTPMT1 or Ptpmt1 were cloned using *Bsm*BI restriction site. All oligonucleotide sequences were listed in Table S4. pLKO.1-Puro or pLentiGuide-Puro were introduced into cancer cells by lentiviral transduction approach. Cells infected with pLKO.1-Puro and pLentiGuide-Puro vectors were selected by 1 μg/ml puromycin (Sigma-Aldrich).

Mouse models

All animal experiments were approved by the Committee on the Use of Live Animals in Teaching and Research, the University of Hong Kong and conducted according to the Animals (Control of Experiments) Ordinance of Hong Kong. All mice were fed with normal chow diet under the maintenance and care of the Centre for Comparative Medicine Research (CCMR), HKU Li Ka Shing Faculty of Medicine. For orthotopic implantation model, 1.5×10^6 luciferase-labeled MHCC97L-Cas9-EV, -sgPTPMT1-1 and -sgPTPMT1-2 subclones were suspended in 15 μL Matrigel (BD Bioscience) and injected into the left lobes of the livers of 6- to 8-week-old male BALB/c nude mice. For PTPMT1 inhibition, AD (0.5 mg/kg/day) were administrated by intraperitoneal injection 15 days after inoculation and the mice were euthanized on day 42. 100 mg/kg D-luciferin (Gold Biotechnology) was administered to the tumor-bearing mice by IP injection and bioluminescent imaging was performed by Xenogen IVIS a100 Imaging System (Caliper). Lung tissues were harvested for *ex vivo* bioluminescent imaging. Liver and lung tissues were fixed in 10% formalin. H&E analysis and histological analysis were performed. For hydrodynamic tail vein injection (HDTVi) model, two plasmid DNA mixtures were used: 1) p53 KO by CRISPR-Cas9-KO plasmid and c-Myc OE by Sleeping Beauty (SB) transposon system plasmid; 2) p53 KO and Ptpmt1 by CRISPR-Cas9-KO plasmid and c-Myc OE by Sleeping Beauty (SB). Oligo sequences of sgPtpmt1 is listed in Table S4. The plasmids were added to saline at a volume of 10% body weight and injected into the blood stream of 6- to 8-week-old male C57BL/6N mice in 6-8 s. For PTPMT1 inhibition, AD (0.5 mg/kg/day) were administrated by IP injection 14 days after inoculation and the mice were euthanized on day 32. Livers were harvested and tumor volumes were measured by an electronic caliper with the following formula: length (mm) x width (mm) x depth (mm) x 0.52. Liver tissues were then fixed by 10% formalin for histological analysis. For subcutaneous injection model, 1×10^6 MHCC97L or 2×10^6 HCT116 suspended in a volume of 100 μL (50 μL Matrigel, 50 μL PBS) were injected into both sides of the flanks of 6- to 8-week-old male BALB/c nude mice. For MHCC97L model, AD (0.5 mg/kg/day) was administrated 16 days after inoculation and the mice were euthanized on day 35. For HCT116 model, AD (0.5 mg/kg/day) was administrated starting from the day of subcutaneous injection and the mice were euthanized on day 19. Tumor volumes and weights of the mice were monitored starting from the first day of AD treatment. Tumor volumes were measured by an electronic caliper and calculated using the following formula: length (mm) x width (mm) x depth (mm) x 0.52. For ovarian cancer mouse model, 1×10^6 luciferase labeled ES-2 cells were resuspended in 100 μL PBS and injected intraperitoneally into the peritoneal cavity of 6- to 8-week-old female BALB/c NUDE mice. AD (0.5 mg/kg/day) was administrated starting from the day of inoculation and the mice were euthanized on day 16. 100 mg/kg D-luciferin was administered to the mice by IP injection for bioluminescent imaging. Pancreas and omentum as well as intestines and mesenterium were harvested for *ex vivo* bioluminescent imaging and fixed in 10% formalin. H&E analysis and histological analysis were performed.

Patient samples

The use of human tissue samples was approved by the Institutional Review Board of the University of Hong Kong/Hospital Authority Hong Kong West Cluster. Human liver tumors and corresponding paired nontumorous (NT) liver samples were collected during surgical resection at Queen Mary Hospital, the University of Hong Kong (QMH-HKU). The liver tissue samples were snap-frozen in liquid nitrogen and stored at −80°C. Prior acknowledgments from patients were obtained by signed consent for collection and usage of resected liver tissues. For the sample size, 60 and 49 cases of human HCC and non-tumorous liver (NT) tissues from QMH-HKU cohort and TCGA database respectively were used to evaluate the expression values of PTPMT1 mRNA. For allocation of PTPMT1 high and low experimental groups, HCC tissues with PTPMT1 expression >5 FPKM were considered as high expression (according to the best expression cut-off algorithm in the Human Protein Altas database). HCC tissues with PMTPT1 expression $\leq$ 5 FPKM were considered as low expression. Survival analyses were done with Kaplan-Meier curve and log-rank test. Number of cases in overall survival analysis (n = 365); Number of cases in disease free survival analysis (n = 312).

METHOD DETAILS

CRISPR-Cas9 library screening

The Human GeCKO v2A CRISPR-Cas9 knockout pooled library (Addgene) was a gift from Prof. Feng Zhang (Board Institute) (Sanjana et al., 2014). The GeCKO v2A library contains 65,386 sgRNAs targeting a total of 19,052 human genes and 1864 human miRNAs (3 sgRNAs for each gene, 4 sgRNAs for each miRNA and 1000 non-targeting controls (NTCs) was first transduced by lentiviral approach

into MHCC97L with stable Cas9 protein expression. A low MOI (~0.3) was used to ensure efficient barcoding of each cell with one sgRNA. After selection by 1.6 μg/ml of puromycin (Sigma-Aldrich) for 7 days, the mutant cell pool was cultured in 20% O_2 or 1% O_2 for another 7 days. Culture medium was replenished every day. In order to achieve 400x coverage of the GeCKO v2A library, at least of 3×10^7 cells were collected for genomic DNA (gDNA) extraction followed by sgRNA PCR amplification using NEBNext® High-Fidelity 2X PCR Master Mix (New England Biolabs). Subsequently, high-throughput amplicon sequencing of the PCR products was performed by Novogene. sgRNA read count was analyzed by MAGeCK v0.5.7 software (Li et al., 2014).

Quantitative real-time PCR

TRIzol® reagent (Ambion®) was used for total RNA extraction. GeneAmp Gold RNA PCR Core Kit (Applied Biosystems) was used for cDNA preparation. Quantitative real-time PCR of PTPMT1 in HCC cells was performed with SYBR Green qPCR Master Mix (Applied Biosystems). Primer sequences were listed in Table S5. RT-qPCR amplifications of PTPMT1 and 18S (internal control) were performed on human HCC clinical samples using the Taqman® Gene Expression Assay (Applied Biosystems).

Drugs and chemicals

A stock solution of Alexidine dihydrochloride, AD (Cayman), was prepared in DMSO at 10 mM. Working concentrations of these reagents are indicated in figure legends of individual experiments. For *in vivo* experiments, AD in PEGE-400 (Sigma-Aldrich) and equal amount of vehicle were injected into animals intraperitoneally. Stock solutions of antioxidants N-acetyl-L-cysteine (NAC) (Sigma-Aldrich) and L-glutathione reduced (GSH) (Sigma-Aldrich) were dissolved in H_2O to 100 mM and 500 mM respectively. Tert-Butyl hydroperoxide (tBHP) was dissolved in PBS.

Western blotting

Whole-cell lysate extraction was performed by radio immunoprecipitation assay lysis (RIPA) buffer supplemented with cOmplete™ protease inhibitor (Roche) and PhosSTOP phosphatase inhibitor cocktails (Roche). NDUFA4 and NDUFA4L2 were resolved by 12.5% (vol/vol) sodium dodecyl sulfate - polyacrylamide gel electrophoresis (SDS/PAGE). PTPMT1, Ptpmt1 and β-actin were resolved by 10% (vol/vol) SDS/PAGE. Proteins were transferred onto PVDF membranes (GE Healthcare) by Trans-Blot Turbo Transfer System (Bio-Rad). The following antibodies were used in this study: anti-PTPMT1 antibody (The Human Protein Atlas), anti-Ptpmt1 antibody (Proteintech), anti-NDUFA4L2 antibody (Abcam) and anti-β-actin antibody (Sigma-Aldrich).

Immunofluorescence imaging

5×10^5 MHCC97L-Cas9-EV, -sgPTPMT1-1 and -sgPTPMT1-2 were seeded on glass coverslips in 12-well cell culture plate. Cells were stained with 100 nM MitoTracker Red FM (Thermo Fisher Scientific) and fixed in 4% formalin at room temperature for 15 min. Cells were permeated by 1:1000 Triton X-100 (Sigma-Aldrich) and blocked by 5% FBS in PBST. Cells were then incubated in anti-PTPMT1 antibody (The Human Protein Atlas) overnight. Cells were stained with Alexa Flour 488 conjugated secondary antibody, followed by DAPI (Abcam) staining. Stained slides were mounted and scanned by Zeiss LSM 780 multiphoton laser scanning microscope (Carl Zeiss) with Axiocam microscope camera (Carl Zeiss). Fluorescence images were captured by ZEN microscope software (ZEISS ZEN) and analyzed by ImageJ (Java). For imaging mitochondrial cristae, cells were plated on Mattak Confocal Dish and exposed to 20% O_2 and 1% O_2 for 48 h. NAO (200 nM) was added to cells for 1 h. Cells were imaged by Carl Zeiss LSM 880/900 with Airyscan. Processed Airyscan images were deconvoluted using ZEN software (Blue version). Mitochondrial quantification was performed using ImageJ software. At least 500-600 mitochondria were analyzed for each experimental group.

Transmission electron microscopy

1×10^6 MHCC97L, MHCC97L-Cas9-EV, -sgPTPMT1-1 and -sgPTPMT1-2 subclones were seeded in 10 cm cell culture dish and incubated in 20% O_2 or 1% O_2 for 48 h. Cells were washed by pre-chilled PBS on ice and immediately fixed by pre-chilled 4% formaldehyde overnight at 4°C. Fixed cells were then scrapped on ice, centrifuged at 1500 rpm for 3 min 4°C and resuspended in 1.5 mL 4% formaldehyde. Cell were fixed by 1% OsO_4 for 1 h, dehydrated with a gradient of increasing ethanol concentration and infiltrated in EMBed 812: proylene oxide (2:1) overnight. Cells were then embedded in capsules and heated at 60°C in oven for 24 h. Blocks were trimmed at 0.5 μm thickness, stained with uranyl acetate and lead citrate at room temperature. Cells were imaged with Philips CM100Transmission Electron Microscope with Olympus SIS Tengra CCD Camera (2.3k x 2.3k pixel).

Oxygen consumption rate measurement

Oxygen consumption rates (OCRs) of MHCC97L, MHCC97L-Cas9-EV, -sgPTPMT1-1 and -sgPTPMT1-2 subclones were measured by XFp Cell Mito Stress Test (Aligent) according to manufacturer's protocol. 1×10^4 MHCC97L, MHCC97L-Cas9-EV, -sgPTPMT1-1 and -sgPTPMT1-2 subclones were seeded onto miniplates and incubated in 20% O_2 or 1% O_2 for 48 h. 1 μM oligomycin (complex V inhibitor), 0.5 μM FCCP (disrupts mitochondrial membrane potential) and 0.5 μM rotenone (complex I inhibitor)-antimycin A (complex III inhibitor) mixture were added to wells at sequential time points. Oxygen consumption rate was quantified by Seahorse XFp Analyzer (Aligent). Basal respiration, ATP-linked respiration, proton lead, and maximal respiration were calculated by the Seahorse XF Report Generator (Aligent).

ROS and mitochondrial membrane potential measurement

1×10^5 MHCC97L and 2×10^5 MHCC97L-Cas9-EV, -sgPTPMT1-1 and -sgPTPMT1-2 subclones were seeded onto 6-well cell culture plates. Cells were incubated in 20% O_2 or 1% O_2 for 48 h. For mitochondrial membrane potential measurement, cells were stained with 2 μM 5,5′,6,6'-tetrachloro-1,1',3,3′-tetraethyl-benzimidazolylcarbocyanine chloride (JC-1, Invitrogen) for 15 min at 37°C, scrapped and suspended in 0.5 mL PBS for flow cytometric analysis. For ROS assay, trypsinized cells were stained with 2 μM ROS indicator chloromethyl-20,70-dichlorodihydrofluorescein diacetate (CM-H_2DCFDA, Life Technologies) dissolved in PBS for flow cytometric analysis. For mitochondrial ROS measurement, cells were stained with 20 μM MitoPY1 (Tocris Bioscience) dissolved in PBS for 1 h at 37°C for flow cytometric analysis. Flow cytometer BD LSRFortessa cell analyzer (BD Bioscience) was employed and data were analyzed by Flowjo software (Flowjo).

Mass spectrometry-based lipidomics analysis

Lipids were extracted from MHCC97L-Cas9-EV, -sgPTPMT1-1 and -sgPTPMT1-2 subclones and MHCC97L cells treated with Ctrl and 2 μM AD cultured in 20% O_2 or 1% O_2 for 48 h using a two-step chloroform/methanol protocol (Ejsing et al., 2009). The cells were scraped in PBS and spiked with an internal lipid standard mixture containing: cardiolipin 14:0/14:0/14:0/14:0 (CL), ceramide 18:1;2/17:0 (Cer), diacylglycerol 17:0/17:0 (DAG), hexosylceramide 18:1;2/12:0 (HexCer), lyso-phosphatidate 17:0 (LPA), lyso-phosphatidylcholine 12:0(LPC), lyso-phosphatidylethanolamine 17:1 (LPE), lyso-phosphatidylglycerol 17:1(LPG), lyso-phosphatidylinositol 17:1 (LPI), lyso-phosphatidylserine 17:1 (LPS), phosphatidate 17:0/17:0 (PA), phosphatidylcholine 17:0/17:0 (PC), phosphatidylethanolamine 17:0/17:0 (PE), phosphatidylglycerol 17:0/17:0 (PG), phosphatidylinositol 16:0/16:0 (PI), phosphatidylserine 17:0/17:0 (PS), cholesterol ester 20:0 (CE), sphingomyelin 18:1;2/12:0;0 (SM), sulfatide d18:1;2/12:0;0 (Sulf), triacylglycerol 17:0/17:0/17:0 (TAG). After extraction, the organic phase was transferred to an infusion plate and dried in a speed vacuum concentrator. First step dry extract was re-suspended in 7.5 mM ammonium acetate in chloroform/methanol/propanol (1:2:4, V:V:V). Second step dry extract was re-suspended in 33% ethanol solution of methylamine in chloroform/methanol (0.003:5:1; V:V:V). All liquid handling steps were performed using Hamilton Robotics STARlet robotic platform with the Anti Droplet Control feature for organic solvents pipetting. For profiling, mass spectrometry-based lipid analysis was performed by Lipotype GmbH (Dresden, Germany) as described(Sampaio et al., 2011). Samples were analyzed by direct infusion on a QExactive mass spectrometer (Thermo Scientific) equipped with a TriVersa NanoMate ion source (Advion Biosciences). Data were analyzed with in-house developed lipid identification software based on LipidXplorer (Herzog et al., 2012; Herzog et al., 2011). Data post-processing and normalization were performed using an in-house developed data management system. Only lipid identifications with a signal-to-noise ratio > 5, and a signal intensity 5-fold higher than in corresponding blank samples were considered for further data analysis. The data were imported into MetaboAnalyst 4.0 (https://www.metaboanalyst.ca/) for multivariate analysis.

For targeted lipid analysis of phosphatidylglycerol (PG) and cardiolipin (CL), the lipids were extracted as above with a CL internal standard mixture 1 (Avanti LM6003): CL 24:1/24:1/24:1/14:1; CL 14:1/14:1/14:1/15:1; CL 15:0/15:0/15:0/16:1; CL22:1/22:1/22:1/14:1. The samples were analyzed in negative ionization mode on ultra-performance liquid chromatography (UPLC) coupled to a QTRAP 6500+ tandem mass spectrometer (Applied Biosystems, Foster City, CA) equipped with electrospray source with a ACQUITY UPLC BEH C18 column (100 × 2.1 mm i.d., 1.7 μm particle size) (Waters Corporation, Milford Massachusetts, U.S.A.). The lipid was washed out isocratically with a mobile phase consisting of 0.1% ammonium hydroxide in acetonitrile/water (90:10, v/v) at a flow rate of 0.4 mL/min as previously reported (Xu et al., 2018). MRM was used for analysis and the MS transition of the analyzed CL and PG were listed in supplementary material. Data acquisition and analysis were performed with the instrument's SCIEX QS software.

Mitochondrial CL level detection

Mitochondria of MHCC97L, MHCC97L-Cas9-EV, -sgPTPMT1-1 and -sgPTPMT1-2 subclones were isolated by Mitochondria Isolation Kit (Thermo Fisher Scientific). After culturing cells in in 20% O_2 or 1% O_2 for 48 h, 2×10^6 cells were harvested, and mitochondria was isolated according to the manufacturer's protocol. Enriched mitochondrial fractions were then used for CL detection by Cardiolipin Assay Kit (BioVision) in 96-well white plates with flat bottom. CL standard curve was generated using CL reconstituted by CL Assay Buffer. Probe was reconstituted in CL Assay Buffer, added to each well and incubated at room temperature for 5 min. Fluorescence was recorded at Ex/Em 340/480 nm using Synergy H1 Hybrid Multi-Mode Reader (BioTek). Calculation of CL concentration is as follow: C = B / V x D (nmol /ml) (B = amount of CL in the sample well from Standard Curve (nmol); V = volume of sample added into the well; D = dilution factor).

Cell proliferation assay

2×10^4 MHCC97L-Cas9-EV, -sgPTPMT1-1 and -sgPTPMT1-2 subclones were seeded onto 12-well cell culture plate and placed in 20% O_2 or 1% O_2 for up to 96 h. Cells were trypsinized and resuspended in DMEM-HG supplemented with 10% FBS and 1% penicillin-streptomycin and immediately counted by TC10 Automated Cell Counter (Bio-Rad) using cell counting slides (Bio-Rad) every other day up to 4 days.

Immunohistochemistry

Human and mouse tissues were fixed in 10% formalin and washed by 70% ethanol before paraffin embedding. Deparaffinization was performed with xylene and subsequently with ethanol for tissue rehydration. Tissue sections were boiled in 1 mM EDTA buffer for

antigen retrieval, immersed in 3% H_2O_2 in 1X TBS for endogenous peroxidase quenching followed by incubation with primary antibodies (anti-PTPMT1 antibody (The Human Protein Atlas) and anti-Ptpmt1 antibody (Proteintech) overnight at 4°C. Slides were then incubated in horseradish peroxidase-conjugated secondary Abs (Dako) for 30 min at room temperature, developed by 3,3′-diaminobenzidine (DAB) (Sigma-Aldrich) and counterstained by hematoxylin. Tissues were dehydrated by ethanol and re-mounted on slides. Slides were scanned by NanoZoomer S210 Digital slide scanner (Hamamatsu) and analyzed by NDP.view2 Viewing software (Hamamatsu).

Cell viability assay

1×10^3 MHCC97L, Hep3B, Huh7 and HepG2 were seeded onto 96-well cell culture plate per well in a final volume of 100 μl incubated in 20% O_2 or 1% O_2 for up to 7 days. Cell viability was determined with Cell Proliferation Kit II (XTT) (Roche). XTT labeling master mix was prepared by mixing XTT labeling reagent and electron coupling regent at a ratio of 50:1. 50 μl XTT labeling master mix were then added to each well and the cells were incubated for 30 min at 37°C. Absorbance was measured once every 30 min up to 3 h at 450 nm by Infinite® F200 plate reader (Tecan).

Cell apoptosis assay

2×10^5 MHCC97L-Cas9-EV, -sgPTPMT1-1 and -sgPTPMT1-2 subclones were seeded onto 6-well cell culture plates. For AD treatment, MHCC97L cells were incubated either in 20% O_2 or 1% O_2, or in Ctrl or 200 μM tBHP (Thermo Fisher Scientific) for 24 h. For MHCC97L-Cas9-EV, -sgPTPMT1-1 and -sgPTPMT1-2 subclones, cells were incubated either in 20% O_2 or 1% O_2, or in Ctrl or 200 μM tBHP (Thermo Fisher Scientific) for 48 h. All floating and adhered cells were collected and stained with propidium iodide (Calbiochem) and Annexin V (MBL International Corporation). Flow cytometric analysis was performed by BD LSRFortessa cell analyzer (BD Bioscience) and flow data were analyzed by Flowjo software (Flowjo).

The Cancer Genome Atlas

Transcriptome sequencing results with mRNA expression levels of PTPMT1 from 49 pairs of human HCC tissues with the corresponding nontumorous (NT) liver tissues were retrieved from The Cancer Genome Atlas (TCGA) database through cBioPortal (http://www.cbioportal.org/). The prognostic significance of PTPMT1 overexpression was determined by the Kaplan-Meier method followed by the log-rank test.

QUANTIFICATION AND STATISTICAL ANALYSIS

GraphPad Prism 7.0 software (GraphPad Software) was used for statistical analyses. Student's t test was used for most experiments unless indicated. Data on graph are representative of 3 independent experiments ($n = 3$). Data are expressed as mean ± SEM $p < 0.05$ is considered statistically significant.